Voltage Instability Analysis Using P-V or Q-V Analysis

by

Weili Yi

A Thesis Presented in Partial Fulfillment
of the Requirements for the Degree
Master of Science

Approved April 2017 by the
Graduate Supervisory Committee:

Vijay Vittal, Co-Chair
Daniel Tylavsky, Co-Chair
Jiangchao Qin

ARIZONA STATE UNIVERSITY

May 2017

ABSTRACT

In the recent past, due to regulatory hurdles and the inability to expand transmission systems, the bulk power system is increasingly being operated close to its limits. Among the various phenomenon encountered, static voltage stability has received increased attention among electric utilities. One approach to investigate static voltage stability is to run a set of power flow simulations and derive the voltage stability limit based on the analysis of power flow results. Power flow problems are formulated as a set of nonlinear algebraic equations usually solved by iterative methods. The most commonly used method is the Newton-Raphson method. However, at the static voltage stability limit, the Jacobian becomes singular. Hence, the power flow solution may fail to converge close to the true limit.

To carefully examine the limitations of conventional power flow software packages in determining voltage stability limits, two lines of research are pursued in this study. The first line of the research is to investigate the capability of different power flow solution techniques, such as conventional power flow and non-iterative power flow techniques to obtain the voltage collapse point. The software packages used in this study include Newton-based methods contained in PSSE, PSLF, PSAT, PowerWorld, VSAT and a non-iterative technique known as the holomorphic embedding method (HEM).

The second line is to investigate the impact of the available control options and solution parameter settings that can be utilized to obtain solutions closer to the voltage collapse point. Such as the starting point, generator reactive power limits, shunt device control modes, area interchange control, and other such parameters.

ACKNOWLEDGEMENTS

First of all, I would like to express my sincere appreciation and gratitude to my co-chairs, Dr. Vittal and Dr. Tylavsky, for their invaluable guidance and support throughout the graduate experience. Dr. Vittal has always been a great source of encouragement and inspiration. His sharp engineering insight into problems and dedication to profession and perfection always impress me. I do appreciate the time working with Dr. Tylavsky. I am always impressed by his patience and responsibility towards his students. Without their guidance, I could not continue to improve my research work.

Secondly, I would like to grateful and sincerely thank my committee member, Dr. Qin for all the inspiring discussions and guidance. I would also like to express my gratitude to the Electric Power Research Institute (EPRI) for the financial support.

Last but not least, I want to thank my parents for their love and endless support. I would also like to thank my colleagues and friends, especially Shruti Rao, Yujia Zhu, Nan Li and Xingpeng Li for their help and guidance. I enjoyed the days I spent at Arizona State University.

TABLE OF CONTENTS

Page

CHAPTER Page

CHAPTER Page

LIST OF TABLES

Table Page

Table Page

Table Page

LIST OF FIGURES

Figure Page

Figure Page

NOMENCLATURE

B_{kj}	Susceptance of Y_{kj}
CPF	Continuation power flow
ERCOT	Electric Reliability Council of Texas
G_{kj}	Conductance of Y_{kj}
HEM	Holomorphic embedding method
I_k	Phasor current injection at bus k
$\boldsymbol{J}$	Jacobian matrix
$\boldsymbol{J}_{Aug}$	Augmented Jacobian matrix
$\boldsymbol{J}_{\boldsymbol{R}}$	Reduced Jacobian matrix
K	Generation and load scaling factor
P_k	Active power injection at bus k
$P_{Generation,k}$	Active power generation at bus k
$P_{Load,k}$	Active power load at bus k
Q_k	Reactive power injection at bus k
$Q_{Generation,k}$	Reactive power generation at bus k
$Q_{Load,k}$	Reactive power load at bus k
Q_{Gmax}	Maximum reactive power generation
Q_{Gmin}	Minimum reactive power generation
S_k	Complex power injection at bus k
SVS	Static VAr system
$\boldsymbol{T}$	CPF tangent vector
$\boldsymbol{t}$	CPF normalized tangent vector
VAr	Volt-ampere reactive

Y_{kj}	Mutual admittance between bus j and bus k
Y_{kk}	Self admittance of bus k
α	HEM power scaling factor
δ_k	Voltage phase angle at bus k
θ_{kj}	Phase angle of Y_{kj}
λ	CPF power scaling factor
$\boldsymbol{\Lambda}$	Diagonal eigenvalue matrix of the reduced Jacobian matrix
$\boldsymbol{\eta}$	Left eigenvalue matrix of the reduced Jacobian matrix
$\boldsymbol{\xi}$	Right eigenvector matrix of the reduced Jacobian matrix

CHAPTER 1

INTRODUCTION

1.1 Overview

As the active power and the reactive power load in a system or an area of the system increases, the system approaches its power transfer limit. There also exists a possibility of the system having less reactive power reserves. If the system is too close to its static stability limits, a small disturbance or a further increase in load could result in voltage collapse. Power flow analysis can provide valuable insights into the voltage stability phenomenon. Based on the power flow study results, the weak areas and the weak buses of the system can be found. The power flow solution may fail to converge close to the stability limit. Beyond the stability limit, there is no feasible solution and the power flow solver will diverge. However, many other reasons can lead to convergence failure in the power flow solvers, before the true stability limit is reached. Such as inappropriate power flow solution parameters settings and improper power flow solution control adjustments.

As a result, it is crucial to understand the impacts of the power flow solution techniques, power flow solution parameters and power flow solution control parameters on the power flow simulations and the voltage stability analysis.

1.2 Literature Review

Voltage stability is defined as the ability of a power system to maintain steady voltages at all buses in the system after being subjected to a disturbance from a given initial operating condition [1]. An IEEE/CIGRE joint task force report provides Figure 1-1[1] to classify the stability problem categories and subcategories.

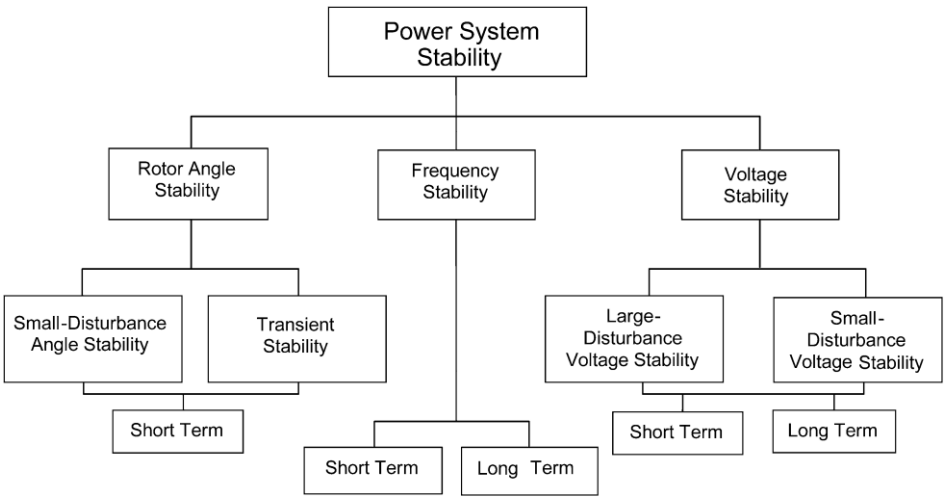

Figure 1-1 Power system stability classification [1]

Voltage stability events span a ranging in time from a few cycles to minutes. Based on the different time frames, [2] gives a classification of voltage stability into two categories. Namely, transient voltage stability and long-term voltage stability. The time frame of transient voltage stability is zero to ten seconds. Since this is also the time frame of rotor-angle stability, a clear identification of the cause and effect relationship between transient voltage stability and rotor-angle stability is hard to achieve if voltage stability is interlinked with rotor-angle stability. The time frame of long-term voltage stability is often several minutes [2]. Reference [3] gives the power system stability classification based on both the time frame and the driving force of the instability. Voltage instability is categorized as being load-driven.

Reference [4] classifies the voltage stability into two subclasses, large-disturbance voltage stability and small-disturbance stability. The ability to maintain all of the bus voltage magnitudes at acceptable steady-state levels following a large disturbance is referred to as large-disturbance voltage stability. The disturbance can be an outage of a key component, such as transformer, generator, inter tie line or system faults. Large-disturbance

voltage stability study mainly focuses on the system nonlinear dynamic performance. The typical approach to study the large-disturbance voltage stability is to run time domain simulation under different scenarios. Small-disturbance voltage stability is the ability to control the voltages following small perturbations. Since the nature of the small-disturbance stability is a steady-state problem, a static approach can be applied to analyze the small-disturbance voltage stability problem.

There are two main methods to study the voltage stability problem. One is the dynamic approach, the other one is the static approach. The dynamic approach can provide a more accurate simulation compared to the static approach. But a detailed description of the system and robust computer software with sophisticated modeling of the power system components are required to run an accurate time-domain simulations [5], [6]. In addition, dynamic simulations cannot provide the sensitivity and degree of instability related information [7]. To study a certain voltage instability situation, the scenarios for dynamic simulations should be carefully selected. On the other hand, the static approach can examine a wide range of system conditions. Additionally, the static approach only requires the solution of algebraic equations, which makes it more computational efficient then the dynamic approach [8].

References [9], [10] introduce the *V*-*Q* sensitivity analysis method for the long-term voltage stability analysis. Mathematically, the *V*-*Q* sensitivity analysis is based on the Jacobian matrix. The disadvantages of *V*-*Q* analysis are the inefficiency and the inaccuracy. The *V*-*Q* sensitivity analysis method only involves local evaluation and a large number of *V*-*Q* curves may be needed to study the overall system performance. The case study in [11] shows that the *V*-*Q* analysis can be misleading sometimes.

Modal analysis was proposed as an analytical tool which can provide system wide information and capability of predicting and quantifying stability margins to evaluate the system voltage stability [12]. The eigenvalue of the reduced Jacobian matrix can be used as an indicator to show which modes the system could be unstable and the magnitude of the eigenvalue is a metric that can be used to estimate the stability margin. Additionally, the eigenvector corresponding to that eigenvalue can provide insight about which areas and components are involved.

1.3 Motivation of Study

Typically, power system voltage stability studies start with an initial steady state operating condition. These initial conditions are normally obtained from power flow programs' solution. The scope of this thesis is to analyze the impacts of the power flow solution parameters and power flow control parameters on various power flow programs. Based on the investigations, the capabilities of different power flow solution techniques and general rules for selecting power flow solution parameters and control parameters as well as the corresponding suggestions and guidelines will be developed. The thesis also provides guidelines to obtain converged power flow solutions as close to the static voltage stability limit as possible and then verifies that the solution obtained is indeed close to the voltage stability using modal analysis.

1.4 Thesis Organization

This thesis has been organized into six chapters.

Chapter 2 introduces the power flow problem and power flow solution methods. The available power flow solution methods in the different software packages are introduced

as well. The general rules for selecting the appropriate solution methods are also discussed.

Chapter 3 introduces the voltage stability analysis methods which include determination of the system maximum load level, modal analysis and the continuation power flow. The analysis results of the test systems are given to identify the weak areas of the test systems.

Chapter 4 illustrates the impact of the power flow solution parameters and power flow control parameters. The simulation results are given to verify the impact of the starting point, generator reactive power limits, switched shunts control and the area interchange control.

Chapter 5 presents a case study of Texas system which focuses on the area interchange control. The area interchange control's impact on the static voltage stability limit is investigated using modal analysis.

Chapter 6 draws the conclusions of the entire study.

CHAPTER 2

POWER FLOW SOLUTION METHODS

2.1 Introduction

The power-flow solution to obtain the steady-state operating conditions of a power system is a nonlinear problem which usually requires iterative methods to find the solution. The Gauss-Seidel method was employed to solve the power flow problem starting from the 1950s [13]. The primary drawback of the Gauss-Seidel method is the exploding computation time and its convergence difficulty. Especially when the Gauss-Seidel method is applied to a large system.

Later, the Newton-Raphson method, which has a quadratic convergence rate, was developed to solve the power flow problem. The computation time increases linearly with the system size [14]. In the standard Newton method, the Jacobian has to be updated at every iteration which could be unnecessary and time consuming. Using sparse-matrix techniques, the Newton-Raphson method fully exploited the sparsity in power systems and provided the power flow solutions in an efficient manner [14].

A modified Newton method was developed to avoid the repeated calculation of the Jacobian, which is the standard fast decoupled method (XB method) [15] (see Section 2.2.4 for details). A few requirements have to be satisfied to achieve more accurate solutions. First, the voltage magnitude for all buses should be around nominal values. Second, the angle differences across the branch should be relatively small. Third, the R/X ratio should not be very large [16]. For most practical cases, the first and second requirement are satisfied. However, the third requirement is not always satisfied.

Reference [17] proposed a modified fast decoupled algorithm. Instead of ignoring the

resistance while building the $\boldsymbol{B}'$ matrix, the resistance is ignored while building $\boldsymbol{B}''$ matrix in the modified fast decoupled algorithm (these matrices are defined in Section 2.2.4). The modified fast-decoupled method converges faster than the standard fast-decoupled method for high R/X ratio systems. Also, the modified fast-decoupled method can solve some cases which cannot be solved by the standard fast-decoupled method. The convergence characteristics of the fast-decoupled method are adversely affected if the coupling between active power and reactive power becomes stronger. The coupling between active power and reactive power will increase when the loading of system is high or if the R/X ratio is high. The BX method can deal with a relatively high R/X ratio, but heavy load can still cause problems with convergence.

2.2 Power Flow Problem and Power Flow Solution

2.2.1 Power Flow Problem

The power flow problem is a well-known problem in the field of power systems engineering, where voltage magnitudes and angles for one set of buses are desired, given that the voltage magnitudes and power levels for another set of buses are known and that a model of the network configuration (unit commitment and circuit topology) is available. There are three types of buses in the power system:

PV bus (Voltage-controlled bus): P and V are specified for PV buses, Q and δ need to be solved. Buses associated with generators, switched shunts, synchronous condensers and static VAr systems are considered as PV buses. The maximum and minimum reactive power limits of this equipment also needs to be specified.

PQ bus (Load bus): P and Q are specified for PQ buses, V and δ need to be solved.

Swing bus (Slack bus): V and δ are specified for the slack bus, P and Q need to be solved. There is only one swing bus in a system. The active power and reactive power losses are usually supplied by the swing bus generator.

where

P is the active power injection at a bus

Q is the reactive power injection at a bus

V is the voltage at a bus

δ is the voltage phase angle at a bus

The net active and reactive power injection at bus k are defined as:

$$P_k = P_{Generation,k} - P_{Load,k} \tag{2.1}$$

$$Q_k = Q_{Generation,k} - Q_{Load,k} \tag{2.2}$$

The complex power injection at bus k can be given by:

$$S_k = P_k + jQ_k = V_k I_k^* \tag{2.3}$$

The network equations which represent the relationship between the bus voltage and current can be written as:

$$\boldsymbol{I} = \boldsymbol{Y_{bus}} \boldsymbol{V} \tag{2.4}$$

Where $\boldsymbol{I}$ is the source current injection vector and $\boldsymbol{V}$ is the bus voltage vector.

Network equations also can be written as:

$$\begin{bmatrix} I_1 \\ I_2 \\ \cdots \\ I_n \end{bmatrix} = \begin{bmatrix} Y_{11} & Y_{12} & \ldots & Y_{n1} \\ Y_{21} & Y_{22} & \ldots & Y_{2n} \\ \ldots & \ldots & \ldots & \ldots \\ Y_{n1} & Y_{n2} & \ldots & Y_{nn} \end{bmatrix} \begin{bmatrix} V_1 \\ V_2 \\ \cdots \\ V_n \end{bmatrix} \tag{2.5}$$

where

n is the total number of buses

V_k is the bus voltage at bus k

I_k is the phasor current injection at bus k

Y_{kj} is the mutual admittance between bus j and bus k

Y_{kk} is the self admittance of bus k

The k^{th} row in (2.5) is:

$$I_k = \sum_{j=1}^{n} Y_{kj} V_j \tag{2.6}$$

The power injection equations can be written as:

$$P_k + jQ_k = V_k \left[\sum_{j=1}^{n} Y_{kj} V_j \right]^* , \quad k = 1, 2, \dots, \mathrm{n} \tag{2.7}$$

From (2.7), the power balance equation at bus k can be written as:

$$P_k = |V_k| \sum_{j=1}^{n} |Y_{kj}| \, |V_j| \cos(\delta_k - \delta_j - \theta_{kj}) \tag{2.8}$$

$$Q_k = |V_k| \sum_{j=1}^{n} |Y_{kj}| \, |V_j| \sin(\delta_k - \delta_j - \theta_{kj}) \tag{2.9}$$

Y_{kj} can be expressed in rectangular coordinates as:

$$Y_{kj} = G_{kj} + jB_{kj} \tag{2.10}$$

Now, the power balance equation can be rewritten as:

$$P_k = |V_k| \sum_{j=1}^{n} |V_j| [G_{kj} \, cos(\delta_k - \delta_j) + B_{kj} sin(\delta_k - \delta_j)] \tag{2.11}$$

$$Q_k = |V_k| \sum_{j=1}^{n} |V_j| \, [G_{kj} sin(\delta_k - \delta_j) - B_{kj} cos(\delta_k - \delta_j)] \tag{2.12}$$

2.2.2 Gauss-Seidel Method

The Gauss-Seidel method can be applied to solve (2.3) and (2.5), the iterative process is as follows:

$$V_k(i+1) = \frac{1}{Y_{kk}}\left[I_k - \sum_{j=1}^{k-1} Y_{kj}V_j(i+1) - \sum_{j=k+1}^{n} Y_{kj}V_j(i)\right] \tag{2.13}$$

Since the current can be given by:

$$I_k = \frac{P_k - jQ_k}{V_k^*} \tag{2.14}$$

Equation (2.13) can be rewritten as:

$$V_k(i+1) = \frac{1}{Y_{kk}}\left[\frac{P_k - jQ_k}{V_k^*(i)} - \sum_{j=1}^{k-1} Y_{kj}V_j(i+1) - \sum_{j=k+1}^{n} Y_{kj}V_j(i)\right] \tag{2.15}$$

The reactive power injection. Q_k, is unknown for a PV bus, but it can be calculated by (2.9) or (2.12):

$$Q_k = |V_k(i)| \sum_{j=1}^{n} \left|V_j(i)\right| \left[G_{kj}sin\big(\delta_k(i) - \delta_j(i)\big) - B_{kj}cos\big(\delta_k(i) - \delta_j(i)\big)\right] \tag{2.16}$$

From (2.2), the reactive power generation at bus k is:

$$Q_{Generation,k} = Q_k + Q_{Load,k} \tag{2.17}$$

$Q_{Generation,k}$ needs to be checked for every iteration. If $Q_{Generation,k}$ exceeds the limit Q_{Gmax} or Q_{Gmin}, the bus type will change from PV bus to PQ bus and $Q_{Generation,k}$ is fixed at its limit for next iteration. Likewise, all generators on VAr limits should be checked at each iteration to see if they have come off of VAr limits.

The stopping criteria for the Gauss-Seidel method is usually established by setting a limit on the voltage magnitude change between successive iterations to be smaller than a

specified tolerance ε:

$$\left|\frac{|V_k(i+1)| - |V_k(i)|}{|V_k(i)|}\right| < \varepsilon \tag{2.18}$$

The computation requirement for a single iteration in the Gauss-Seidel method is acceptable. But the rate of convergence is linear for the Gauss-Seidel method. When the system is large, the computational burden is significant. Another drawback of the Gauss-Seidel method is that (2.15) cannot be exactly applied to PV buses. Since the reactive power generation is unknown for PV buses. Reactive power will be calculated by using the best guess of the voltage magnitudes in equation (2.16). Thus, this process deteriorates the convergence of the Gauss-Seidel method. The Gauss-Seidel method is useful when the starting point of the power flow case is unknown or other methods diverge with the existing start point. Hence, it is occasionally used as a means to reliably start the power flow solution. After a few iterations, the algorithm is switched from the Gauss-Seidel method to the Newton method or to the fast-decoupled method.

2.2.3 Newton-Raphson Method

The steps of the Newton method include:

Step 1: Calculate the $\Delta \boldsymbol{P}(i)$ and $\Delta \boldsymbol{Q}(i)$ for i^{th} iteration, starting with $\boldsymbol{x}(0)$,

$$\begin{bmatrix}\Delta \boldsymbol{P}(i) \\ \Delta \boldsymbol{Q}(i)\end{bmatrix} = \begin{bmatrix}\boldsymbol{P} - \boldsymbol{P}[\boldsymbol{x}(i)] \\ \boldsymbol{Q} - \boldsymbol{Q}[\boldsymbol{x}(i)]\end{bmatrix} \tag{2.19}$$

where

$$\boldsymbol{x}(i) = \begin{bmatrix}\boldsymbol{\delta}(i) \\ \boldsymbol{V}(i)\end{bmatrix} \tag{2.20}$$

Step 2: Calculate the Jacobian matrix

The Jacobian matrix is given by:

$$\boldsymbol{J} = \begin{bmatrix} \begin{bmatrix} \frac{\partial P_1}{\partial \delta_1} & \cdots & \frac{\partial P_1}{\partial \delta_n} \\ \vdots & \ddots & \vdots \\ \frac{\partial P_n}{\partial \delta_1} & \cdots & \frac{\partial P_n}{\partial \delta_n} \end{bmatrix} & \begin{bmatrix} \frac{\partial P_1}{\partial V_1} & \cdots & \frac{\partial P_1}{\partial V_n} \\ \vdots & \ddots & \vdots \\ \frac{\partial P_n}{\partial V_1} & \cdots & \frac{\partial P_n}{\partial V_n} \end{bmatrix} \\ \begin{bmatrix} \frac{\partial Q_1}{\partial \delta_1} & \cdots & \frac{\partial Q_1}{\partial \delta_n} \\ \vdots & \ddots & \vdots \\ \frac{\partial Q_n}{\partial \delta_1} & \cdots & \frac{\partial Q_n}{\partial \delta_n} \end{bmatrix} & \begin{bmatrix} \frac{\partial Q_1}{\partial V_1} & \cdots & \frac{\partial Q_1}{\partial V_n} \\ \vdots & \ddots & \vdots \\ \frac{\partial Q_n}{\partial V_1} & \cdots & \frac{\partial Q_n}{\partial V_n} \end{bmatrix} \end{bmatrix} \tag{2.21}$$

Where $j \neq k$:

$$\frac{\partial P_k}{\partial \delta_j} = |V_k|\left|Y_{kj}\right|\left|V_j\right| sin(\delta_k - \delta_j - \theta_{kj})$$

$$\frac{\partial P_k}{\partial V_j} = |V_k|\left|Y_{kj}\right| cos(\delta_k - \delta_j - \theta_{kj})$$

$$\frac{\partial Q_k}{\partial \delta_j} = -|V_k|\left|Y_{kj}\right|\left|V_j\right| cos(\delta_k - \delta_j - \theta_{kj})$$

$$\frac{\partial Q_k}{\partial V_j} = |V_k|\left|Y_{kj}\right| sin(\delta_k - \delta_j - \theta_{kj})$$

Or where $j = k$:

$$\frac{\partial P_k}{\partial \delta_j} = -|V_k| \sum_{\substack{j=1 \\ j \neq k}}^{n} \left|Y_{kj}\right| \left|V_j\right| sin(\delta_k - \delta_j - \theta_{kj})$$

$$\frac{\partial P_k}{\partial V_j} = |V_k||Y_{kk}| \cos\theta_{kk} + \sum_{j=1}^{n} \left|Y_{kj}\right| \left|V_j\right| cos(\delta_k - \delta_j - \theta_{kj})$$

$$\frac{\partial Q_k}{\partial \delta_j} = |V_k| \sum_{\substack{j=1 \\ j \neq k}}^{n} \left|Y_{kj}\right| \left|V_j\right| cos(\delta_k - \delta_j - \theta_{kj})$$

$$\frac{\partial Q_k}{\partial V_j} = -|V_k||Y_{kk}|\, sin\, \theta_{kk} + \sum_{j=1}^{n} |Y_{kj}|\, |V_j|\, sin(\delta_k - \delta_j - \theta_{kj})$$

Step 3: Solve the following equation to obtain the vector $\begin{bmatrix}\Delta\boldsymbol{\delta}(i)\\ \Delta\boldsymbol{V}(i)\end{bmatrix}$:

$$\boldsymbol{J}\begin{bmatrix}\Delta\boldsymbol{\delta}(i)\\ \Delta\boldsymbol{V}(i)\end{bmatrix} = \begin{bmatrix}\Delta\boldsymbol{P}(i)\\ \Delta\boldsymbol{Q}(i)\end{bmatrix} \tag{2.22}$$

Step 4: Calculate the $\boldsymbol{x}(i+1)$:

$$\boldsymbol{x}(i+1) = \begin{bmatrix}\boldsymbol{\delta}(i+1)\\ \boldsymbol{V}(i+1)\end{bmatrix} = \begin{bmatrix}\boldsymbol{\delta}(i)\\ \boldsymbol{V}(i)\end{bmatrix} + \begin{bmatrix}\Delta\boldsymbol{\delta}(i)\\ \Delta\boldsymbol{V}(i)\end{bmatrix} \tag{2.23}$$

Unlike the Gauss-Seidel method, the stopping criteria for the Newton's method is usually based on the power mismatches instead of the voltage magnitude mismatches. When the power mismatches for all buses are smaller than a specified convergence tolerance, a converged solution is reached. $Q_{Generation,k}$ needs to be checked for every iteration. If $Q_{Generation,k}$ exceeds the limit Q_{Gmax} or Q_{Gmin}, the bus type will be changed from PV bus to PQ bus and $Q_{Generation,k}$ will be fixed at its limit in next iteration. Likewise, all generators on VAr limits should be checked at each iteration to see if they have come off of VAr limits.

Due to the quadratic convergence of the Newton-Raphson method, it only takes a few iterations to reach the solution. The number of iterations to reach the solution is not sensitive to the size of the system. The Newton-Raphson method requires fewer iterations than the Gauss-Seidel and the fast-decoupled method. But the computation time for each iteration is longer than the Gauss-Seidel and the fast decoupled method. Poor estimation of the starting point and the lack of sufficient reactive power support can result in convergence difficulties with the Newton-Raphson method.

2.2.4 Fast Decoupled Method

In the full Newton-Raphson method, the Jacobian has to be updated during every iteration. The computation cost may be unacceptable for some online studies, especially with large networks. Based on the active power-power angle and reactive power-voltage magnitude decoupling principle, references [17] proposed the fast decoupled method to solve the power flow problem. The coupling between *P*-*V* and *Q*-*δ* are ignored to accelerate the calculation. Hence, (2.22) can be simplified to:

$$\Delta \boldsymbol{P} = \frac{\partial \boldsymbol{P}}{\partial \boldsymbol{\delta}} \Delta \boldsymbol{\delta} = \boldsymbol{H} \Delta \boldsymbol{\delta} \tag{2.24}$$

$$\Delta \boldsymbol{Q} = \frac{\partial \boldsymbol{Q}}{\partial \boldsymbol{V}} \Delta \boldsymbol{V} = \boldsymbol{L} \Delta \boldsymbol{V} \tag{2.25}$$

where for $j \neq k$

$$H_{kj} = \frac{\partial P_k}{\partial \delta_j} = |V_k||V_j|_j \left[G_{kj} sin(\delta_k - \delta_j) - B_{kj} cos(\delta_k - \delta_j)\right] \tag{2.26}$$

$$L_{kj} = \frac{\partial Q_k}{\partial V_j} = |V_k| \left[G_{kj} sin(\delta_k - \delta_j) - B_{kj} cos(\delta_k - \delta_j)\right] \tag{2.27}$$

where for $j = k$

$$H_{kk} = \frac{\partial P_k}{\partial \delta_k} = -B_{kk}|V_k|^2 - Q_k \tag{2.28}$$

$$L_{kk} = \frac{\partial Q_k}{\partial V_k} = -B_{kk}|V_k| + \frac{Q_k}{|V_k|} \tag{2.29}$$

If the following assumptions which are valid for practical power systems are made as follows:

$$cos\delta_{kj} \approx 1; \quad G_{kj} sin\delta_{kj} \ll B_{kj}; \quad Q_k \ll B_{kk}|V_k|^2$$

Equation (2.26) to (2.29) become:

where for $j \neq k$

$$H_{kj} = \frac{\partial P_k}{\partial \delta_j} \cong -|V_k|\left|V_j\right|_j B_{kj} \tag{2.30}$$

$$L_{kj} = \frac{\partial Q_k}{\partial V_j} \cong -|V_k|\, B_{kj} \tag{2.31}$$

where for $j=k$

$$H_{kk} = \frac{\partial P_k}{\partial \delta_k} \cong -B_{kk}|V_k|^2 \tag{2.32}$$

$$L_{kk} = \frac{\partial Q_k}{\partial V_k} \cong -B_{kk}|V_k| \tag{2.33}$$

Now (2.24) and (2.25) can be simplified to:

$$\Delta \boldsymbol{P} = (\boldsymbol{V}\boldsymbol{B}'\boldsymbol{V})\Delta\boldsymbol{\delta} \tag{2.34}$$

$$\Delta \boldsymbol{Q} = (\boldsymbol{V}\boldsymbol{B}'')\Delta\boldsymbol{V} \tag{2.35}$$

Where $\boldsymbol{B}'$ and $\boldsymbol{B}''$ are identical to the $-\boldsymbol{B}$ and $\boldsymbol{B}$ is the susceptance matrix.

If the series resistance is neglected in the calculation of $\boldsymbol{B}'$, this type of fast decoupled method is called XB method.

If the series resistance is neglected in the calculation of $\boldsymbol{B}''$, this type of fast decoupled method is called BX method.

2.3 Available Solution Methods in Software Packages

Four commercial software packages are used in this study. The name and the version of the packages are shown in Table 2-1:

Table 0-1 Software package information

Software Package	Version	Developer
PSS®E	33	Siemens PTI
PSLF	19	General Electric
PSAT	15	Powertech Labs Inc.
PowerWorld	19	PowerWorld Corporation

2.3.1 PSSE Power Flow Solution Methods

PSSE provides five methods to solve the power flow problem. Namely, Gauss-Seidel method, Modified Gauss-Seidel method, Full Newton-Raphson method, Decoupled Newton-Raphson method and Fixed-Slope Decoupled Newton-Raphson method.

Gauss-Seidel method: The mathematical formulation is shown in Section 2.2.2. The Gauss-Seidel method usually shows a characteristic of slow convergence. Hence, an acceleration factor is usually applied to accelerate the calculation. The Gauss-Seidel method only checks the voltage magnitude mismatches during the iterative process. Once the voltage magnitude changes between successive iterations satisfies the convergence tolerance, a converged solution is found. The strength of the Gauss-Seidel method is that a poor estimation of voltage can be used as a starting point. The method is tolerant of operating conditions which have inadequate reactive power support.

Modified Gauss-Seidel method: The Gauss-Seidel method cannot handle negative reactance branches [18]. A low impedance branch may cause slow convergence. The difference between the Gauss-Seidel method and Modified Gauss-Seidel is that Modified Gauss-Seidel method is capable of dealing with the negative reactance branches connected to PQ buses [18]. If there is a negative reactance branch which is connected to a PV bus or swing bus, the Modified Gauss-Seidel method is not able to handle it properly [18]. A line

which has impedance less than 0.0001pu is usually treated as a zero impedance branch in other algorithms, but the Modified Gauss-Seidel method will not treat such a line as a zero impedance line. Other settings, such as acceleration factors, convergence tolerance and blowup threshold are similar to those used with the Gauss-Seidel method.

Full Newton-Raphson method: Mathematical formulation is shown in Section 2.2.3.

Decoupled Newton-Raphson method: Based on (2.24) and (2.25), the *P-δ* calculation in the Decoupled Newton-Raphson method is decoupled from the *Q-V* calculation. Every iteration can be separated into two parts. The first half of the iteration is used to calculate the $\boldsymbol{\delta}$ with the fixed bus voltage magnitudes $|\boldsymbol{V}|$, the second half is using the new $\boldsymbol{\delta}$ to update $|\boldsymbol{V}|$ [18].

Fixed-Slope Decoupled Newton-Raphson method: Similar to the Decoupled Newton-Raphson method, the *P-δ* calculation is decoupled from the *Q-V*. Moreover, the simplified Jacobian is almost unchanged during the calculation. The *P-δ* matrix $\boldsymbol{B'}$ stays fixed, and *Q-V* matrix $\boldsymbol{B''}$ will be updated only when a bus type switching occurs.

2.3.2 PSLF Power Flow Solution Methods

PSLF only provides the full Newton method to solve the power flow problem.

2.3.3 PSAT Power Flow Solution Methods

PSAT provides four methods to solve the power flow problem. Auto, Newton-Raphson, Fast Decoupled (XB) and Fast Decoupled (BX). The Gauss-based methods are not available in PSAT.

Auto: When the solution algorithm is selected as Auto, PSAT will apply standard Fast Decoupled (XB) method to solve the power flow. When the real and reactive power

mismatches are smaller than 1 MW/MVAr, PSAT will switch the algorithm from the fast-decoupled method to the Newton-Raphson method [19].

Newton-Raphson: The mathematical formulation is shown in Section 2.2.3. PSAT provides the standard Newton-Raphson method.

Fast Decoupled (XB): The mathematical formulation is shown in Section 2.2.4. PSAT provides the standard fast decoupled method which named as Fast Decoupled XB.

Fast Decoupled (BX): The mathematical formulation is shown in Section 2.2.4. This is the modified fast-decoupled method. The BX method is preferred to XB method when there ae some high R/X ratio lines in the system.

2.3.4 PowerWorld Power Flow Solution Methods

PowerWorld provides three methods to solve the power flow problem. Full Newton method, Polar NR Power Flow method and Fast Decoupled method. Before solving the problem, PowerWorld makes a pre-processing check for voltage angle, voltage magnitude, low branch impedance and generator output. PowerWorld solves the power flow problem in three nested loops [20]. Inner loop: Power Flow Loop. Conventional power flow problem is solved in this loop. Middle loop: Control Loop. After the inner loop is solved, middle loop will check the control devices setting and make proper adjustment. Outer loop: MW Control Loop. Check the active power balance in the system and adjust dispatch with area control or island-based control.

2.4 Holomorphic Embedding Method

Because the iterative methods may fail to converge or obtain a solution near the voltage collapse point, the need existed for a method which could obtain a solution when the bus

voltages are relatively low. The Holomorphic Embedding Method (HEM) was introduced in power flow studies by A. Trias in 2011 to overcome this problem. HEM can guarantee the solution up to the voltage collapse point in a non-iterative and deterministic computation approach if the solution exists [21].

For an *n* bus system, all buses except slack bus, can be divided into 3 sets:

Set *m*: consists of PQ buses

Set *p*: consists of PV buses that are not on the reactive power limits

Set *q*: consists of PV buses that are on reactive power limits

The conventional power balance equations written in current balance form for PQ buses are:

$$\sum_{j=1}^{n} Y_{kj} V_j = \frac{S_k^*}{V_k^*}, \quad k \in m \tag{2.36}$$

Power balance equations of PV buses on reactive power limits are similar to that of the PQ bus power balance equations. The conventional power balance equations for PV buses that are not on reactive power limits are given by:

$$P_k = Re\left(\sum_{j=1}^{n} Y_{kj}^* V_j^*\right), \quad k \in p \tag{2.37}$$

$$|V_k| = V_k^{sp}, \quad k \in p \tag{2.38}$$

Where V_k^{sp} is the specified voltage magnitude at bus *k*.

One way to holomorphically embed the power-flow problem is to embed the power balance equations with a scaling factor, α. The power balance equations become:

$$\sum_{j=1}^{n} Y_{kj}\, V_j(\alpha) = \frac{\alpha S_k^*}{V_k^*(\alpha^*)}, \quad k \in m \tag{2.39}$$

$$\sum_{j=1}^{n} Y_{kj}\, V_j(\alpha) = \frac{\alpha\left(P_{gk} - P_{lk}\right) - j(Q_{gk}(\alpha) - \alpha Q_{lk})}{V_k^*(\alpha^*)}, \quad k \in p \tag{2.40}$$

$$\sum_{j=1}^{n} Y_{kj}\, V_j(\alpha) = \frac{\alpha\left(P_{gk} - P_{lk}\right) - j(Q_{gk\_limit} - \alpha Q_{lk})}{V_k^*(\alpha^*)}, \quad k \in q \tag{2.41}$$

where

P_{gk} is the active power generation at bus k

$Q_{gk}(\alpha)$ is the reactive power generation at bus k

P_{lk} is the active power load at bus k

Q_{lk} is the reactive power load at bus k

Q_{gk_limit} is the PV bus reactive power generation limit at bus k

The voltage constraints are:

$$V_k(\alpha) \cdot V_k^*(\alpha^*) = \left|V_k^{sp}\right|, \quad k \in p \tag{2.42}$$

$$V_k(\alpha) = V_k^{sp}, \quad k \in slack\ bus$$

The power injection equations at bus k are:

$$P_k = P_{gk} - P_{lk}, \quad k \in p \tag{2.43}$$

$$Q_k(\alpha) = Q_{gk}(\alpha) - Q_{lk}, \quad k \in p \tag{2.44}$$

The power balance equations can be rewritten as:

$$\sum_{j=1}^{n} Y_{kj}\, V_j(\alpha) = \frac{\alpha P_k - j(Q_{gk}(\alpha) - \alpha Q_{lk})}{V_k^*(\alpha^*)}, \quad k \in p \tag{2.45}$$

$$\sum_{j=1}^{n} Y_{kj} V_j(\alpha) = \frac{\alpha P_k - j(Q_{gk\_limit} - \alpha Q_{lk})}{V_k^*(\alpha^*)}, \quad k \in q \tag{2.46}$$

$\boldsymbol{V}(\alpha)$ and $Q_{gk}(\alpha)$ can be represented by power series, since they are holomrophic in the scaling parameter α:

$$V(\alpha) = V[0] + V[1]\alpha + \cdots + V[n](\alpha)^n \tag{2.47}$$

$$Q_{gk}(\alpha) = Q_{gk}[0] + Q_{gk}[1]\alpha + \cdots + Q_{gk}[n](\alpha)^n \tag{2.48}$$

$$V^*(\alpha^*) = V^*[0] + V^*[1]\alpha + \cdots + V^*[n](\alpha)^n \tag{2.49}$$

The formulation above will allow the active power and reactive power of loads, and the active power generation of generators to be scaled by α. The reactive power generation of PV buses are functions of α. Power series coefficients are solved by substituting $\boldsymbol{V}(\alpha)$ and $Q_{gk}(\alpha)$ in the power balance equations. The coefficient of α^i on the left-hand side of the power balance equations should be equal to the coefficient of α^i on the right-hand side of the power balance equations. More details can be found in [22]. However, the power-series radius of convergence cannot guarantee that the series converges over the entire domain of the function. Hence, the maximal analytic continuation of the power series, the Padé approximant, is introduced to guarantee that the solution found by HEM is the high voltage solution [23, 24]. The Padé approximant is given by:

$$V(\alpha)_{\text{Padé}} = \frac{a_0 + a_1\alpha + a_2\alpha^2 + \cdots + a_L\alpha^L}{b_0 + b_1\alpha + b_2\alpha^2 + \cdots + b_L\alpha^M} \tag{2.50}$$

Once the Padé approximant is obtained, the power flow solution at different load levels can be found by varying the load scaling factor α in the Padé approximant instead of resolving the power flow problem.

The strength of the HEM method is that the convergence is guaranteed if the solution

exists. Once the Padé approximant is achieved, it is not necessary to resolve the power flow problem under different load levels. Instead, one just needs to use different load scaling parameters α to calculate the bus voltages and reactive power generations.

The available HEM program used for this study has been developed by Professor Tylavsky at Arizona State University and his students.

2.5 Power Flow Solution Methods Summary and test Systems

In some cases, it is hard to solve the power flow with a single method. More than one method can be applied to these cases to find a converged solution.

In general, the Gauss method is more tolerant in cases which have trouble allocating reactive power and have a poor voltage profile. But the Gauss method could have poor convergence if the system is close to its active power active power transfer limit. On the other hand, the Newton's method is more tolerant of cases which have trouble with transferring active power. But the Newton's method could have poor convergence if the system has reactive power inadequacy and has a poor voltage profile. The power flow solution may fail to converge if a poor estimation of the voltage is used as a starting point.

The Gauss method is less sensitive to the starting point. But when the solution gets closer to the true solution, the solution will converge more slowly. The Newton's method has a better performance when the solution is near the true solution. Therefore, for a new power-flow case without any previous knowledge, users can start with the Gauss method, and then switch to the Newton's method after few iterations.

The computation time of the fast decoupled method per iteration is less than that of the Newton's method. The fast decoupled method is less sensitive to voltage starting point. However, the fast decoupled method cannot handle a high R/X ratio system properly.

A scaling factor *K* is used to scale both the generation and the load. Both active power and reactive power demand of the load are multiplied by *K*. As a result, the power factor of all loads stay unchanged. The active power output of the generators are multiplied by *K* to scale the generation. The scaling factor *K* is increased in steps to gradually increase the load level until no converged power flow solution can be obtained. The last load level which has a converged power flow solution is considered as the critical case. The scaling factor of the critical case is considered as the critical load scaling factor, critical *K*.

The IEEE 300 bus test system [25] and a synthetic Texas 2007 bus system are used in this study [26]. IEEE 300 bus system contains 69 generators, 304 transmission lines and 197 loads. For the base case, the total active and reactive power generation are 22929.42 MW and 8760.26 MVAr, respectively. The total active and reactive power load are 22469.86 MW and 7572.97 MVAr, respectively. The Texas 2007 bus system contains 282 generators, 2481 transmission lines and 1417 loads. For the base case, the total active and reactive power generation are 50851.56 MW and 10150.55 MVAr, respectively. The active and reactive power load are 49775.55 MW and 14186.02 MVAr, respectively.

2.5.1 PSSE Solution Methods Examples

The number of iterations at base case with VAr limits imposed are given in the following examples. The maximum number of iterations is set as 100. NC 100 in the tables denote that after 100 iterations, there is still no converged solution.

Table 0-2 PSSE IEEE 300 Bus System Base Case Algorithm Comparison

K	Gauss	Modified Gauss	Decoupled	Fixed slope	Full Newton
1	8	5	3	3	2

Table 0-3 PSSE Texas System Base Case Algorithm Comparison

K	Gauss	Modified Gauss	Decoupled	Fixed slope	Full Newton
1	NC 100	NC 100	10	10	3

As shown in Table 2-2 and Table 2-3, due to the quadratic convergence characteristic, the Newton method usually requires less iterations than the Gauss method. The fast decoupled method requires more iterations than the Newton method. The Gauss method cannot determined a converged solution even for the base case condition of the Texas system.

2.5.2 PSAT Solution Methods Examples

If the algorithm option is selected as Auto in PSAT, the fast decoupled method will be applied first. When the largest mismatch for active power and reactive power is smaller than 1 MW or 1 MVAr respectively, then PSAT will switch to the Newton method. The first number in the parentheses gives the number of iterations required for convergence by the fast decoupled method, and the second number in the parentheses indicates the number of iterations required by Newton method. As shown in the results, Newton method usually requires fewer iterations than the fast decoupled method.

Table 0-4 Number of Iterations: PSAT IEEE 300 Bus System Base Case Algorithm Comparison

K	Auto	Newton	XB	BX
1	4 (3+1)	3	4	4

Table 0-5 Number of iterations: PSAT Texas System Base Base Algorithm Comparison

K	Auto	Newton	XB	BX
1	10 (8+2)	5	11	11

2.5.3 PowerWorld Solution Methods Examples

PowerWorld can provide the computation time required to solve the power flow. Although the fast decoupled method takes more iterations than the full Newton method, the total computation time for the fast decoupled method is less than that for the full Newton method as shown in the Table 2-7. Since the Jacobian does not need to be updated at every iteration in the fast decoupled method, the computation time per iteration of the fast decoupled method is much lower than that of the Newton method.

Table 0-6 Number of Iterations: PowerWorld IEEE 300 Bus System Base Case Algorithm Comparison

K	Full Newton	Fast Decoupled
1	2	4

Table 0-7 Number of Iterations: PowerWorld Texas System Base Case Algorithm Comparison

K	Full Newton	Time in seconds	Fast Decoupled	Time in seconds
1	4	0.218	10	0.063

CHAPTER 3

STATIC VOLTAGE STABILITY ANALYSIS

3.1 Introduction

The objective of the voltage stability study is to predict loadability limits in order to avoid voltage collapse and enhance the system voltage stability. Before any countermeasures are taken, the weak areas of the system and the weak buses need to be identified. Voltage instability events can be initiated due to several reasons. Though the process of voltage collapse is a dynamic phenomenon, static network solution methods can be used to produce metrics which are good indicators of voltage stability margin and can identify weak areas or buses of the system. This chapter introduces the steps to identify the weak areas and the weak buses in the system.

3.2 Critical Load Scaling Factor

3.2.1 Critical *K* from Conventional Methods

The critical *K* for the Texas system when VAr limits are imposed at the first iteration in the different software packages are compared in Table 3-1.

Table 0-1 Texas System Critical *K* Comparison

Software	PSSE	PSLF	PSAT	PowerWorld
Critical *K*	1.032	1.032	1.033	1.032

The results from these four packages are very similar, except PSAT gives a slightly higher value. The number of iterations required for convergence by the different power flow solution methods in PSSE are given in Table 3-2. The Gauss method does not obtain

a converged solution. The fast decoupled methods take more iterations than the Newton method.

Table 0-2 Number of Iterations: PSSE Texas System Critical Case Algorithm Comparison

K	Gauss	Modified Gauss	Decoupled	Fixed slope	Full Newton
1.032	NC 100	NC 100	56	57	6

The number of iterations required by the different power flow solution methods tested using PSAT are given in Table 3-3. The fast decoupled methods require more iterations than the Newton method. Notice that the standard fast decoupled method (XB) does not obtain a converged solution, but the BX method can obtain the converged solution. BX method is preferred to the XB method in systems with high R/X ratio, the largest R/X ratio is 0.486621 which occurs on a branch that connects bus 1096 and bus 1105.

Table 0-3 Number of Iterations: PSAT Texas System Critical Case Algorithm Comparison

K	Auto	Newton	XB	BX
1.033	39 (36+3)	7	NC 100	67

The number of iterations taken by the different methods in PSAT are given in Table 3-4. PowerWorld gives the execution time required to solve the power flow problem. The fast decoupled method takes 52 more iterations to obtain the solution, but the total time consumption is less than that of the full Newton method.

Table 0-4 Number of Iterations: PowerWorld Texas System Critical Case Algorithm Comparison

K	Full Newton	Time in seconds	Fast Decoupled	Time in seconds
1.032	6	0.672	58	0.453

3.2.2 HEM Critical *K*

The HEM can give a converged solution for the Texas system up to K=1.16 in which the power mismatches are satisfied but the bus types of some buses are oscillating. The PSSE solution at the critical case is used to examine the convergence of the HEM. If the same set of generators on VAr limits is specified in the HEM, when the loading level reduced to 96.9% of the PSSE critical loading level, the power mismatches will be satisfied with 63 terms in the power series. The HEM can guarantee the convergence at the solution theoretically. However, the bus type switching algorithm and insufficient precision can result in the inability to find the solution in some cases [21]. This behavior is also observed in [21].

3.3 Modal Analysis

B. Gao and P. Kundur proposed a modal analysis approach to evaluate voltage stability for large power systems in 1992 [12]. Based on a linear approximation of the system model, modal analysis calculates the eigenvalue and eigenvector of the reduced Jacobian matrix. Each eigenvalue represents a mode of *V-Q* variation. The magnitude of the eigenvalue can be considered as a quantitative measurement of the static voltage stability margin. The eigenvectors are used to calculate the bus participation factors which indicates the weak areas of the system.

Equation (2.22) can be rewritten as:

$$\begin{bmatrix}\Delta \boldsymbol{P} \\ \Delta \boldsymbol{Q}\end{bmatrix} = \begin{bmatrix}\boldsymbol{J}_{P\delta} & \boldsymbol{J}_{PV} \\ \boldsymbol{J}_{Q\delta} & \boldsymbol{J}_{QV}\end{bmatrix}\begin{bmatrix}\Delta \boldsymbol{\delta} \\ \Delta \boldsymbol{V}\end{bmatrix} \tag{3.1}$$

Because of the weak coupling between $\Delta \boldsymbol{P}$ and $\Delta \boldsymbol{V}$, the following assumption can be made in static analysis:

$$\Delta \boldsymbol{P} = 0$$

$$\begin{bmatrix} \mathbf{0} \\ \Delta \boldsymbol{Q} \end{bmatrix} = \begin{bmatrix} \boldsymbol{J}_{P\delta} & \boldsymbol{J}_{PV} \\ \boldsymbol{J}_{Q\delta} & \boldsymbol{J}_{QV} \end{bmatrix} \begin{bmatrix} \Delta \boldsymbol{\delta} \\ \Delta \boldsymbol{V} \end{bmatrix} \tag{3.2}$$

The above equation can be separated as:

$$0 = \boldsymbol{J}_{P\delta} \Delta \boldsymbol{\delta} + \boldsymbol{J}_{PV} \Delta \boldsymbol{V} \tag{3.3}$$

$$\Delta \boldsymbol{Q} = \boldsymbol{J}_{Q\delta} \Delta \boldsymbol{\delta} + \boldsymbol{J}_{QV} \Delta \boldsymbol{V} \tag{3.4}$$

Substituting $\Delta \boldsymbol{\delta}$ in (3.4):

$$\Delta \boldsymbol{Q} = (\boldsymbol{J}_{QV} - \boldsymbol{J}_{Q\delta} \boldsymbol{J}_{P\delta}^{-1} \boldsymbol{J}_{PV}) \Delta \boldsymbol{V} \tag{3.5}$$

The reduced Jacobian matrix $\boldsymbol{J}_{\boldsymbol{R}}$ can be defined as:

$$\boldsymbol{J}_{\boldsymbol{R}} = \boldsymbol{J}_{QV} - \boldsymbol{J}_{Q\delta} \boldsymbol{J}_{P\delta}^{-1} \boldsymbol{J}_{PV} \tag{3.6}$$

Equation (3.5) becomes:

$$\Delta \boldsymbol{Q} = \boldsymbol{J}_{\boldsymbol{R}} \Delta \boldsymbol{V} \tag{3.7}$$

In the *V*-*Q* analysis, (3.7) can be written as:

$$\Delta \boldsymbol{V} = \boldsymbol{J}_{\boldsymbol{R}}^{-1} \Delta \boldsymbol{Q} \tag{3.8}$$

The diagonal element of $\boldsymbol{J}_{\boldsymbol{R}}^{-1}$ is the sensitivity factor at each bus which is also the slope of the *Q*-*V* curve. A stable operating point requires all sensitivity factors to be positive. A smaller sensitivity factor magnitude indicates a more stable operating point. The system is unstable if at least one sensitivity factor is negative. The decomposition of $\boldsymbol{J}_{\boldsymbol{R}}$ and $\boldsymbol{J}_{\boldsymbol{R}}^{-1}$ are:

$$\boldsymbol{J}_{\boldsymbol{R}} = \boldsymbol{\xi} \boldsymbol{\Lambda} \boldsymbol{\eta} \tag{3.9}$$

$$\boldsymbol{J}_{\boldsymbol{R}}^{-1} = \boldsymbol{\xi} \boldsymbol{\Lambda}^{-1} \boldsymbol{\eta} \tag{3.10}$$

where

$\boldsymbol{\xi}$ is the right eigenvector matrix of the reduced Jacobian matrix

$\boldsymbol{\Lambda}$ is the diagonal eigenvalue matrix of the reduced Jacobian matrix

$\boldsymbol{\eta}$ is the left eigenvector matrix of the reduced Jacobian matrix

Equation (3.8) can be written as:

$$\Delta \boldsymbol{V} = \boldsymbol{\xi} \boldsymbol{\Lambda}^{-1} \boldsymbol{\eta} \Delta \boldsymbol{Q} \tag{3.11}$$

or

$$\Delta \boldsymbol{V} = \sum_{i} \frac{\boldsymbol{\xi}_i \boldsymbol{\eta}_i}{\lambda_i} \Delta \boldsymbol{Q} \tag{3.12}$$

where

$\boldsymbol{\xi}_i$ is the i^{th} column of $\boldsymbol{\xi}$

λ_i is the i^{th} eigenvalue

$\boldsymbol{\eta}_i$ is the i^{th} row of $\boldsymbol{\eta}$

Equation (3.12) describes the *Q-V* response of each mode. The sign and magnitude of λ_i provide a qualitative measure of system stability. A positive λ_i indicates that the incremental change in voltage magnitude of bus *i* is along the direction of the incremental change in reactive power injection at bus *i*. Hence, the system is at a stable operating condition if λ_i is positive. A negative λ_i indicates that the incremental change in voltage magnitude of bus *i* is along the opposite direction of the incremental change in reactive power injection at bus *i*. Hence, the system is at an unstable operating condition if λ_i is negative. The incremental change in voltage magnitude is inversely proportional to the magnitude of the λ_i times the incremental change in reactive power injection. A smaller positive λ_i indicates that a small amount of reactive power injection change could result in a dramatically large change in voltage magnitude. Therefore, the larger the λ_i, the more stable the system. A value of $\lambda_i = 0$ indicates a voltage collapse since any variation in reactive power injection gives infinite change in voltage magnitude.

In (3.12), if the $\Delta \boldsymbol{Q}$ is assumed to have only one non-zero element which is the k^{th} element, and the value of this non-zero element is unity, then, (3.12) becomes:

$$\Delta \boldsymbol{V} = \sum_i \frac{\boldsymbol{\xi}_i \eta_{ik}}{\lambda_i} \tag{3.13}$$

The V-Q sensitivity analysis at bus k gives:

$$\frac{\boldsymbol{\partial} V_k}{\boldsymbol{\partial} Q_k} = \sum_i \frac{\xi_{ki} \eta_{ik}}{\lambda_i} \tag{3.14}$$

Compared to the *V-Q* sensitivity analysis, modal analysis is able to capture the voltage magnitude change at all buses due to a reactive power injection change at bus k.

In mode i, the participation of bus k is defined by:

$$Bus\ Participation\ Factor_{ki} = \xi_{ki} \eta_{ik} \tag{3.15}$$

where

ξ_{ki} is the k^{th} element of $\boldsymbol{\xi}_i$

η_{ik} is the k^{th} element of $\boldsymbol{\eta}_i$

Recall from (3.12), that $\xi_{ki} \eta_{ik}$ describe the contribution of λ_i to a *Q-V* response at bus k in mode i. The buses with relatively large bus participation factors for the smallest eigenvalue (mode) determine the weak areas. Reactive power compensation can be applied at buses that have large bus participation factors. Bus participation factors can show the type of the mode. There are two types of modes in general, local modes and non-localized modes. A local mode has few buses with large participation factors and other bus participation factors close to zero. A non-localized mode has many buses that have large bus participation factors and other bus participation factors close to zero.

Modal analysis using eigenvalue and eigenvector analysis can identify the weak region

of the system. The bus participation factors show the critical region associated with each mode. The smallest eigenvalue of the reduced Jacobian matrix indicates the nearness of the system to a voltage stability boundary. The modal analysis result for the Texas system at critical case is given in Table 3-5.

Table 0-5 Modal Analysis at K=1.032

No.	Bus	Gen	Part.Fac.	Voltage
1	1668	QL	1.00000	0.9246
2	1532	QL	0.95166	0.8878
3	6		0.80054	0.8836
4	31		0.79661	0.8814
5	182		0.79347	0.8889
6	350		0.79236	0.8727
7	346		0.78725	0.8745
8	34		0.78683	0.8661
9	156		0.78599	0.8915
10	153		0.78055	0.8923
11	154		0.77822	0.9127
12	1667	QL	0.77472	0.9246
13	347		0.76887	0.8742
14	36		0.76271	0.8791
15	18		0.76069	0.8805
16	181		0.75929	0.9204
17	1670	QL	0.75907	0.9246
18	41		0.75616	0.8666
19	119		0.75256	0.9009
20	33		0.75143	0.8682

The mode 1 results indicate that bus 1668 is a weak bus. PSSE can plot a diagram to show the system topology around a selected bus. This can be very helpful in determining how far the low voltage bus is from other generator buses. The topology diagram starting with the bus 1668 as level 1 can be plotted in PSSE, as shown in Figure 3-1.

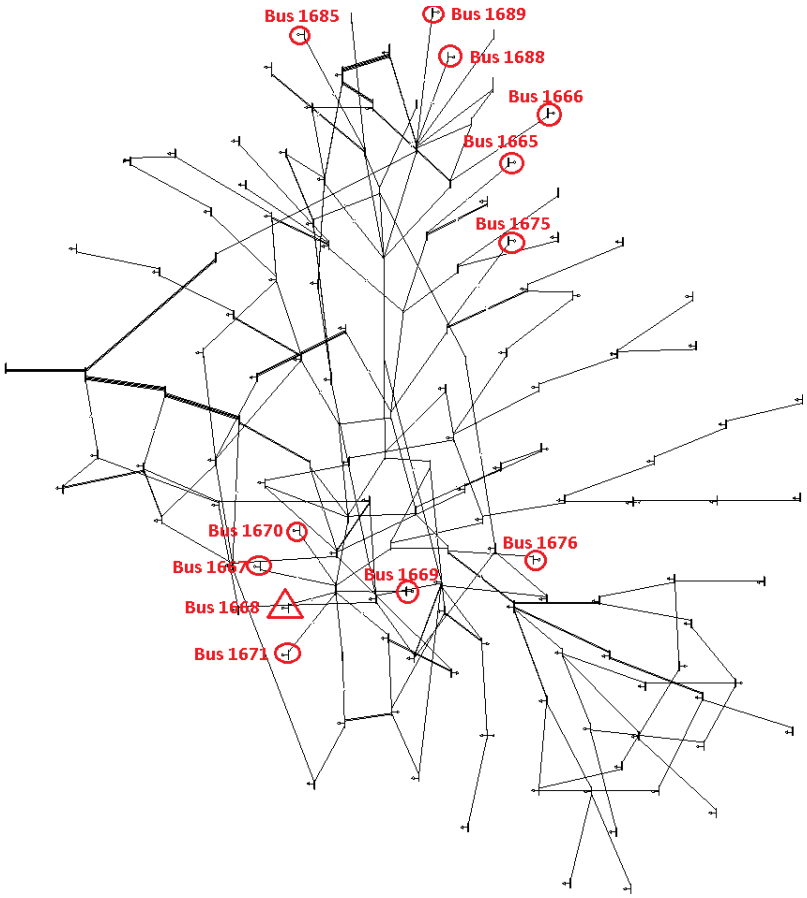

Figure 0-1 Bus 1668 Region Topology Diagram

There are 7 levels in the diagram. Generators are marked in red in Figure 3-2. All the generator outputs and bus voltage *magnitudes* are given in Table 3-6. As shown in the table, all the generators nearby have reached their VAr limits.

Table 0-6 Generators near Bus 1668

Bus	Q_{Gen}	Q_{Max}	$V_{Scheduled}$	V_{Actual}	Level
1668	0	0	1.04	0.9067	1
1667	0.8	0.8	1.04	0.9231	2
1669	0	0	1.04	0.8998	2
1670	0.9	0.9	1.04	0.9231	2
1671	100.1	100.1	1.04	0.9249	2
1676	518.2	518.2	1.04	0.9827	4
1675	198.6	198.6	1.04	0.9395	6
1665	273.9	273.9	1.01	0.9869	7
1666	216.1	216.1	1.04	0.9233	7
1688	0	0	1.04	0.9067	7
1689	208.9	208.9	1.04	0.9316	7

The same situation can be observed at bus 34. The lowest bus voltage magnitude for the entire system is at bus 34. Bus 34 is in mode 1 and has a large bus participation factor. Figure 3-3 shows the system topology near the bus 34.

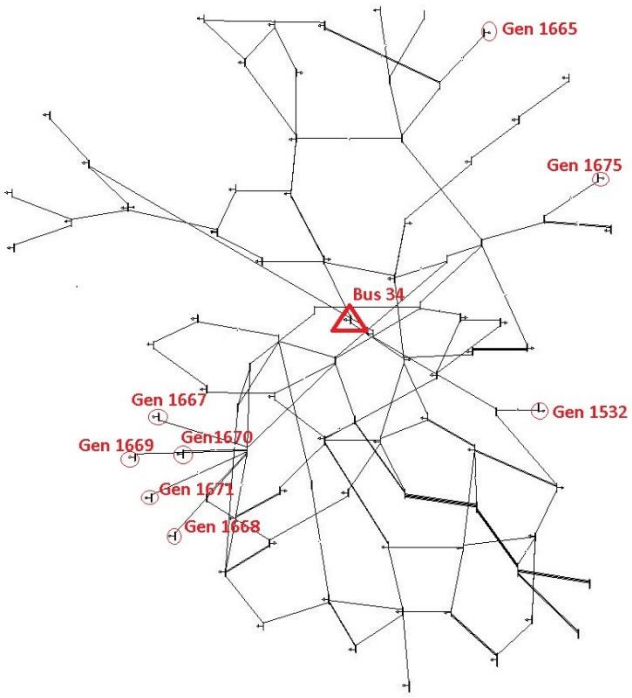

Figure 0-2 Bus 34 Region Topology Diagram

No generator bus can be found even if the topology diagram is extended up to 6 levels. The generators that show up at the 6th level are listed in Table 3-7. There are no reactive power sources near bus 34, which explains the low voltage problem at bus 34.

Table 0-7 Generators near Bus 34

Bus	Q_{Gen}	Q_{Max}	$V_{Scheduled}$	V_{Actual}
1532	0.5	0.5	1.04	0.8862
1665	273.9	273.9	1.01	0.9869
1667	0.8	0.8	1.04	0.9231
1668	0.4	0.4	1.04	0.9231
1669	0	0	1.04	0.8998
1670	0.9	0.9	1.04	0.9231
1671	100.1	100.1	1.04	0.9249
1675	198.6	198.6	1.04	0.9395

3.4 Continuation Power Flow

Continuation Power Flow (CPF) was proposed by V. Ajjarapu in 1992 [27]. It is a

numerical technique to trace the solution branch near the bifurcation point using a path-following methodology [28]. The predictor-corrector scheme is adopted to capture the path-following feature. The CPF algorithm overcomes the Jacobian singularity problem by reformulating the power flow problem with locally parametrized continuation techniques [29].

The power flow problem can be represented by a set of nonlinear equation:

$$\boldsymbol{F}(\boldsymbol{x}) = \boldsymbol{0} \tag{3.16}$$

where

$$\boldsymbol{x} = [\boldsymbol{\delta}, \boldsymbol{V}]^{\boldsymbol{T}} \tag{3.17}$$

The continuation power flow introduces a load parameter, λ, to track the solution of the nonlinear equations. The base case has $\lambda = 0$. The parameterized power flow nonlinear equations can be written as:

$$\boldsymbol{F}(\boldsymbol{x}, \lambda) = \boldsymbol{0} \tag{3.18}$$

The reformulated power balance equations at bus *k* are:

$$\Delta P_k = P_{Gk}(\lambda) - P_{Lk}(\lambda) - P_k \tag{3.19}$$

$$\Delta Q_k = Q_{Gk}(\lambda) - Q_{Lk}(\lambda) - Q_k \tag{3.20}$$

where

$$P_k = |V_k| \sum_{j=1}^{n} |Y_{kj}| \, |V_j| \, cos(\delta_k - \delta_j - \theta_{kj}) \tag{3.21}$$

$$Q_k = |V_k| \sum_{j=1}^{n} |Y_{kj}| \, |V_j| \, sin(\delta_k - \delta_j - \theta_{kj}) \tag{3.22}$$

The modified load and generation at bus *k* are:

$$P_{Lk}(\lambda) = P_{Lk0}[1 + \lambda K_{Lk}] \tag{3.23}$$

$$Q_{Lk}(\lambda) = Q_{Lk0}[1 + \lambda K_{Lk}] \tag{3.24}$$

$$P_{Gk}(\lambda) = P_{Gk0}[1 + \lambda K_{Gk}] \tag{3.25}$$

where

P_{Lk0} and Q_{Lk0} are the original load active power and reactive power respectively

$K_{Lk}$and K_{Gk} specify the rate of change in load and generation at bus *k* respectively

The continuation method which includes the predictor process and corrector process can be employed to solve the nonlinear equations. The predictor process starts with the calculation of the tangent vector. The tangent vector is given by:

$$\boldsymbol{T} = [d\boldsymbol{\delta}, d\boldsymbol{V}, d\lambda]^{\boldsymbol{T}} \tag{3.26}$$

The tangent vector is calculated from:

$$[\boldsymbol{F_{\delta}}, \boldsymbol{F_V}, \boldsymbol{F_{\lambda}}]\boldsymbol{T} = \boldsymbol{0} \tag{3.27}$$

$\boldsymbol{F_{\delta}}, \boldsymbol{F_V}, \boldsymbol{F_{\lambda}}$ are partial derivatives of $\boldsymbol{F}(\boldsymbol{\delta}, \boldsymbol{V}, \lambda)$ with respect to $\boldsymbol{\delta}$, $\boldsymbol{V}$ and λ. The $[\boldsymbol{F_{\delta}}, \boldsymbol{F_V}]$ is nothing but the original Jacobian matrix. The tangent vector has to be normalized in order to guarantee the non-singularity of the augmented Jacobian [30]. Therefore, the augmented Jacobian should satisfy:

$$\begin{bmatrix} \boldsymbol{F_{\delta}} & \boldsymbol{F_V} & \boldsymbol{F_{\lambda}} \\ & \boldsymbol{e_k} & \end{bmatrix} [\boldsymbol{t}] = \begin{bmatrix} \boldsymbol{0} \\ \pm 1 \end{bmatrix} \tag{3.28}$$

where $\boldsymbol{e_k}$ is a row vector in which the k^{th} element is the only non-zero element. And the augmented Jacobian is defined as:

$$\boldsymbol{J_{Aug}} = \begin{bmatrix} \boldsymbol{F_{\delta}} & \boldsymbol{F_V} & \boldsymbol{F_{\lambda}} \\ & \boldsymbol{e_k} & \end{bmatrix} \tag{3.29}$$

After the tangent vector is obtained, the predicted solution for iteration *i* is given by:

$$\begin{bmatrix} \boldsymbol{\delta}^k_{\boldsymbol{predict}} \\ \boldsymbol{V}^k_{\boldsymbol{predict}} \\ \lambda^k_{\boldsymbol{predict}} \end{bmatrix} = \begin{bmatrix} \boldsymbol{\delta}^{k-1} \\ \boldsymbol{V}^{k-1} \\ \lambda^{k-1} \end{bmatrix} + \sigma \begin{bmatrix} d\boldsymbol{\delta}^{k-1} \\ d\boldsymbol{V}^{k-1} \\ \lambda^{k-1} \end{bmatrix} \tag{3.30}$$

where σ is the designated step size. The index k and the step size should be chosen appropriately. The rules for selecting the values for these two variables are given in [30].

The corrector then is calculated by:

$$\begin{bmatrix} \Delta\boldsymbol{\delta}^k \\ \Delta\boldsymbol{V}^k \\ \Delta\lambda^k \end{bmatrix} = -\boldsymbol{J}^{-1}_{Aug} \begin{bmatrix} \Delta\boldsymbol{f}^k \\ \mathbf{0} \end{bmatrix} \tag{3.31}$$

The solution after the corrector process is given by:

$$\begin{bmatrix} \boldsymbol{\delta}^k \\ \boldsymbol{V}^k \\ \lambda^k \end{bmatrix} = \begin{bmatrix} \boldsymbol{\delta}^k_{\boldsymbol{predict}} \\ \boldsymbol{V}^k_{\boldsymbol{predict}} \\ \lambda^k_{\boldsymbol{predict}} \end{bmatrix} + \begin{bmatrix} \Delta\boldsymbol{\delta}^k \\ \Delta\boldsymbol{V}^k \\ \Delta\lambda^k \end{bmatrix} \tag{3.32}$$

VSAT in DSA-Tools can use the CPF to trace the *P*-*V* curve at the selected buses. MATLAB Power System Analysis Toolbox (MATLAB PSAT) developed by F. Milano also provides the CPF option [31].

3.5 Critical *K* Comparison

Table 3-8 gives the critical *K* values if different methods are used for the IEEE 300 bus system when VAr limits are imposed.

Table 0-8 IEEE 300 Bus System Critical *K* Comparison

Software	PSAT	MATLAB CPF	HEM
Critical *K*	1.0211	1.0452	1.0675

A zero determinant for the Jacobian indicates the maximum load level is reached [32].

As shown in the modal analysis results, the eigenvalues and eigenvectors are close to zero at the PSAT critical loading level. Table 3-8 shows that, the MATLAB CPF gives a higher critical *K* than the PSAT which uses conventional Newton algorithm to solve the power flow problem. The critical *K* obtained from HEM which is a non-iterative method is higher than the MATLAB CPF and PSAT critical *K*. The CPF and HEM were proposed to overcome the Jacobian singularity issue at the power flow critical point in the literatures. This example illustrates that the CPF indeed has an advantage in solving the power flow at the critical point. Also, HEM can guarantee that a solution exists at the critical point. In this example, there is no oscillating behavior in bus type switching in HEM. Hence, it could give a higher critical *K* than the conventional power flow programs. If the HEM-based power flow solution does not converged at a certain level of load and the equations are structured properly, the cause of the non-convergence is that the proposed loading level exceeds the maximum loading level, assuming discrete tap changing and bus type switching are not causing oscillatory behavior. However, in some cases, CPF and HEM may fail to converge at a non-critical loading level due to the control algorithms causing oscillatory behaviors.

3.6 HEM Weak Bus Determination

Reference [22] introduced the sigma method to estimate the SNBP. Considering a two-bus system with a PQ bus and a slack bus, two buses are connected by a line which has impedance of *Z*. The complex power injected at the PQ bus is *S*. If the slack bus has a unit voltage, the σ can be defined as:

$$\sigma = \frac{ZS^*}{|V_0|^2} \tag{3.33}$$

Once the σ is defined, it can be shown that:

$$U = 1 + \frac{\sigma}{U^*} \tag{3.34}$$

Where $U = V/V_0$

The roots of (3.34) are given by:

$$U = \frac{1}{2} \pm \sqrt[2]{\frac{1}{4} + \sigma_R - \sigma_I{}^2} + j\sigma_I \tag{3.35}$$

Where σ_R is the real part of σ and σ_I is the imaginary part of σ.

The radicand in (3.35) must be non-negative to ensure the existence of a high voltage solution. Hence, the index σ can be used to estimate the SNBP of the system. The σ-condition is given by:

$$\frac{1}{4} + \sigma_R - \sigma_I{}^2 \geq 0 \tag{3.36}$$

For a practical system, the slack bus voltage is not necessary to be 1 pu. If the slack bus voltage is assumed to be V_{Slack}. Based on the proposed method in [22]. Equation (3.34) can be modified as:

$$U(\alpha) = 1 + \frac{\sigma(\alpha)}{U^*(\alpha^*)} \tag{3.37}$$

Where

$$U(\alpha) = \frac{V(\alpha)}{V_{Slack}} \tag{3.38}$$

The updated sigma equation can be written as:

$$\sigma(\alpha) = \frac{V(\alpha) \cdot V^*(\alpha^*)}{{V_{Slack}}^2} - \frac{V^*(\alpha^*)}{V_{Slack}} \tag{3.39}$$

Equation (3.37) can be extended to represent the each node of the system as:

$$\frac{V_i(\alpha)}{V_{Slack}} = 1 + \frac{\sigma_i(\alpha) \cdot V_{Slack}}{V_i^*(\alpha^*)} \tag{3.40}$$

where

$$\sigma_i(\alpha) = \sigma_i[0] + \sigma_i[1]\alpha + \sigma_i[2]\alpha^2 + \cdots \tag{3.41}$$

The value of $\sigma_i[0]$ can be calculated by:

$$\sigma_i[0] = \frac{V_i[0]V_i^*[0]}{{V_{Slack}}^2} - \frac{V_i^*[0]}{V_{Slack}} \tag{3.42}$$

The value of $\sigma_i[n]$ can be calculated from:

$$\sigma_i[n] = \frac{\sum_{k=1}^{n} V_i[n]V_i^*[n-k]}{{V_{Slack}}^2} - \frac{V_i^*[n]}{V_{Slack}} \tag{3.43}$$

The SNBP can be estimated by increasing the load scaling factor until the σ-condition is no longer satisfied. Parts of the numerical results of IEEE 118 bus system study are given in Table 3-9 and Table 3-10. The critical *K* given by PSAT is 2.730. Table 3-9 shows the modal analysis mode 1 results at the critical *K*. Table 3-10 shows the first 10 buses that violate the σ-condition as the load scaling factor increased with different thresholds. The bus number and the corresponding critical load scaling factor are given in the table. As shown in the Table 3-10, the first negative radicand using the Padé approximant is given by bus 24 at load scaling factor 2.652. If the threshold is set to -0.01, bus 26 is the first bus which has a radicand less that -0.01 with a critical load scaling factor 2.724. Similar to the Texas system test case, the HEM critical load scaling factor is short of the critical *K*

obtained from the PSAT. The critical load scaling factor potentially can indicate the weakness of each bus. Although the results from the sigma method do not match with the modal analysis results, the sigma method based on σ-condition can give a good estimation of the SNBP.

Table 0-9 Modal Analysis at K=2.7303 of Mode 1

No.	Bus	Gen	Part.Fac.	Voltage
1	38		1.00000	0.7432
2	44		0.93160	0.7648
3	43		0.42442	0.8318
4	45		0.34782	0.8120
5	22		0.10844	0.8307
6	30		0.09453	0.8781
7	21		0.09438	0.8249
8	37		0.04327	0.9458
9	20		0.03540	0.8685
10	39		0.02864	0.9212

Table 0-10 HEM Weak Bus Determination Results

No.	Bus	Critical factor with -0.01 threshold
1	26	2.724
2	2	2.728
3	48	2.728
4	51	2.728
5	74	2.728
6	106	2.728
7	107	2.728
8	109	2.728
9	110	2.728
10	112	2.728

CHAPTER 4

POWER FLOW SOLUTION PARAMETERS AND CONTROL

4.1 Introduction

Power flow programs provide solution parameters and control parameters for users to adjust the solution process. Inappropriate solution parameter settings and control settings can cause convergence difficulty. This chapter present case studies to investigate the impact of available solution parameters and control parameters. Suggestions to tune the parameters also are given in this chapter.

4.1.1 Power Flow Solution Parameters

Common power flow solution parameters include:

Maximum number of iterations: If the number of iterations reaches the specified maximum number of iterations and still no converged solution is achieved, the solution process will be terminated. If a converged solution exists, and given an appropriate starting point, the full Newton-Raphson method usually can find the solution within 20 iterations. If the fast-decoupled method or Gauss-Seidel method is applied, the maximum number of iterations should be set to a higher value.

Number of Iterations before imposing VAr limits: PSSE and PSLF allow the users to adjust this parameter. Reactive power generation limits will be imposed after the specified number of iterations. It is reasonable not to impose the VAr limits at the beginning of the solution process in some cases. Since a poor initial guess of the starting point may cause some generators to bounce on and off their reactive power output limit or even operate beyond their reactive power generation range during the first few iterations.

Solution tolerance for active power and reactive power mismatch: If there is even one bus whose active power and reactive power mismatches are larger than this specified value, the power flow solution is considered to be a non-converged solution. The recommended value of the solution tolerance is 0.1 MVA for a moderate sized system. When the system has a non-convergence issue, 1 MW tolerance is acceptable.

Voltage tolerance: For any voltage controlled bus, the voltage magnitude mismatch should not exceed the voltage tolerance for a converged power flow solution. The recommended value of voltage tolerance is 0.0001 per unit.

Blowup threshold: If the largest bus voltage magnitude change exceeds this value, the solution is considered to be a diverged solution. The solution process is then terminated. The value of the blow up threshold should not be less than 1 per unit. The recommended value of the blow up threshold value is 3 per unit.

The solution tolerance for real and reactive power are set as 0.1MW and 0.1MVAr respectively, for all the software packages used in this project. The voltage magnitude tolerance is set as 0.0001 per unit if this parameter can be modified by users.

4.1.2 Power Flow Control Options

Common power flow control options include flat start, acceleration factor, reactive power limits control, shunt devices control and area interchange control. The available control options in different software packages and the impact of these control options are investigated in this chapter.

4.2 Starting Point

If the flat start option is selected, all bus voltage magnitudes and phase angles for PQ

buses will be set to 1.0 per unit and 0 degree, respectively. Then, the magnitude of swing bus voltage is set to the specified value in the input data. Users should be very careful in using flat start when area interchange control is enabled. By applying the flat start, the phase angles of all the buses, including the area slack buses are set to zero degrees which could result in non-convergence issue. The IEEE 300 bus system and PSSE are used to study the impact of the starting point. Table 4-1 shows the critical *K* values and number of iterations required to arrive at the critical converged solution if the flat start is used. Table 4-2 shows the critical values of *K* and the number of iterations required to arrive at the critical converged solution if the non-flat start is used. In this case, the starting values of voltage magnitudes and phase angles are specified to be the solution obtained at the previous value of *K* in the study.

Table 0-1 Flat Start Critical *K*

Method	Fixed slope decoupled NR	Full NR
Critical point	1.0207	1.0204
Iteration count	14	12

Table 0-2 Non-flat Start Critical *K*

Method	Fixed slope decoupled NR	Full NR
Critical point	1.021	1.023
Iteration count	11	2

Comparing the results in Table 4-1 with that in Table 4-2, for both the fast decoupled method and the full Newton method, a higher critical *K* can be achieved with a non-flat starting point. Also, with a non-flat starting point, fewer number of iterations are required to reach the converged solution

From Table 4-1 it is observed that with a flat start, the critical *K* obtained by the fast

decoupled method is higher than that obtained by the full Newton method. This is a good example to demonstrate that the fast decoupled method is less sensitive to the starting point and that a poor estimation of the starting point can result in convergence difficulties for the full Newton method.

4.3 Acceleration Factor

In PSSE, acceleration factors can be applied to both the Gauss method and the Newton method. The IEEE 300 bus system and PSSE are used to study the impact of the acceleration factor. Table 4-3 shows the critical *K* values and number of iterations required to arrive at the critical converged solution for different acceleration factors (ACCN) with the full Newton method and with a flat start.

Table 0-3 Acceleration Factor Summary

ACCN	0.32	1
Critical point	1.0209	1.0204
Iteration count	25	12

From Table 4-3, it is observed that a smaller acceleration factor gives a higher critical *K* but takes more iterations to reach the final solution.

Normally, it is not necessary to use an acceleration factor larger than 1 when the Newton method is applied. If the voltage magnitude changes are oscillating during successive iterations, the acceleration factor could be too large for this case. If the voltage magnitude changes are relatively small during the successive iterations, a larger acceleration factor can be applied.

4.4 VAr Limit and Bus Type Switching

Generators can hold the bus voltage magnitudes at the scheduled level by regulating the reactive power generation if the VAr limits are not reached. Once the generators reach the VAr limits, the generator buses become PQ buses. The voltage magnitudes cannot be held at their scheduled values, since no more reactive power can be supplied by those generators. If one power plant has multiple generators, the reactive power will be split in proportion to generators' active power output to ensure identical power factors. If there is any VAr limit violation, the reactive power cannot be split properly, a warning message will show up in the message window. As for the swing bus, the voltage magnitude and phase angle are held at specified values. Table 4-4 gives the critical *K* values with and without imposing the VAr limits. The four software packages used give different critical values of *K* and also have different sets of generators on VAr limits.

Table 0-4 IEEE 300 Bus System Critical *K* with VAr Limit

Software package	PSSE	PSLF	PSAT	PowerWorld
Critical *K* with VAr limits	1.0204	1.0615	1.0211	1.0609
Critical *K* without VAr limits	1.3081	1.3077	1.3077	1.3087

If the VAr limits are imposed for the Texas system, the critical value of *K* and the swing generator outputs are given in Table 4-5.

Table 0-5 Texas System Critical *K* with VAr Limit

Software	PSSE	PSLF	PSAT	PowerWorld
Critical *K*	1.032	1.032	1.033	1.032
Swing Bus P_{Gen}	2365.387	2362.7	2390.77	2364.82
Swing Bus Q_{Gen}	1481.949	1461.3	1576.02	1477.91

The results from the four software packages are quite close to each other. PSAT gives a slightly higher critical value of *K*. PSAT also imposes the VAr limit on the swing generator. If this option is checked in PSAT, the critical value of *K* will be 1.01. Since part of the system reactive power losses are assigned to the swing generator, it is reasonable not to impose the VAr limits on the swing generator. The number of generators on their upper and lower limit are given in the Table 4-6.

Table 0-6 Number of Generators on VAr Limits

	PSSE	PSAT	PowerWorld	PSLF
Iteration	6	7	5	9
$= Q_{Max}$	81	82	81	80
$> Q_{Max}$	1	1	1	1
$= Q_{Min}$	5	5	5	7

PSSE and PowerWorld give the same set of generators on their VAr limits. PSAT has one extra generators on its upper limit compared to the PSSE and PowerWorld solution, which is the generator on bus 1541. The power outputs for the generator at bus 1541 are given in Table 4-7. The reactive power generation range is very narrow for this generator. Differences in control logic in software packages can cause this tiny difference.

Table 0-7 Reactive Power Generation at Bus 1541

	Q_{Gen}	Q_{Max}	Q_{Min}
PSAT	12.7	12.7	-3.2
PSSE	7.4	12.7	-3.2

PSLF has one less generator on its VAr limit compared to the PSSE and PowerWorld solutions, which is the generator on bus 1696. The reactive power generation of this

generator is given in Table 4-8. The generator on bus 1696 is a small generator in a power plant called *Throckmort*. The rated capacity of the generator on bus 1696 is 3.5MVA. In the same power plant, there is another generator which has a rated capacity of 470.5 MVA. It is not easy to allocate the reactive power generation in a power plant which has multiple machines with a wide range in capacities. Additionally, the difference in control logic among the software packages can also result in different reactive power allocation. PSLF has a unique approach to deal with this kind of issue, as shown later.

Table 0-8 Reactive Power Generation at Bus 1696

	Q_{Gen}	Q_{Max}	Q_{Min}
PSSE	0.81	0.81	-0.35
PSLF	0.5	0.81	-0.35

Power flow simulations can be conducted one iteration at a time in all four software packages. The number of generators on VAr limits at every iteration are shown in Table 4-9.

Table 0-9 Number of Generators on VAr Limits Details

	PSSE			PSAT			PowerWorld		
Iteration	$=Q_{Max}$	$>Q_{Max}$	$=Q_{Min}$	$=Q_{Max}$	$>Q_{Max}$	$=Q_{Min}$	$=Q_{Max}$	$>Q_{Max}$	$=Q_{Min}$
1	73	0	27	59	0	27	73	7	9
2	78	1	8	74	0	25	79	2	5
3	80	1	5	80	1	6	79	3	5
4	81	1	5	81	1	5	81	1	5
5	81	1	5	82	1	5	81	1	5
6	81	1	5	82	1	5			
7				82	1	5			

PSSE, PSAT, PowerWorld give similar final results regarding the generators which are on VAr limits. But from Table 4-9, it is obvious that these packages use different

approaches to do the bus type switching. In the first iteration, PSAT has only 59 generators on the VAr limits. But PSSE and PowerWorld have 73 generators on VAr limits. Another difference is that PowerWorld allows the generators to operate beyond their VAr limits before the final solution is reached. However, PSSE and PSAT will not allow this to happen if the VAr limits are imposed starting at the first iteration. As different bus type switching algorithms are applied, one cannot expect identical power flow solutions to be achieved from different software packages.

PSLF has a power flow control parameter called *Minimum VAR limit band width*. If the difference between the upper VAr limit and lower VAr limit is smaller than the *Minimum VAR limit band width*, the reactive power output will be fixed at the mid value between zero and the upper VAr limit [33]. The possible reason leading to this assumption could be inappropriate modeling of the reactive power capability of the generators. Table 4-10 shows the Dale power plant generation information from PSSE for the Texas critical case where K=1.032. Table 4-11 shows the generation information from PSLF at the same operating condition.

Table 0-10 PSSE Dale Power Plant Generation

Bus		P_{Gen}	P_{Max}	P_{Min}	Q_{Gen}	Q_{Max}	Q_{Min}
1754	DALE G0	5.1218	9.6	2.88	1.709	2.443	-1.066
1755	DALE G1	2.3478	4.4	1.32	0.7833	1.12	-0.488
1756	DALE G2	497.2424	932	279.6	163.337	217.156	-113.704

Table 0-11 PSLF Dale Power Plant Generation

Bus		P_{Gen}	P_{Max}	P_{Min}	Q_{Gen}	Q_{Max}	Q_{Min}
1754	DALE G0	5.1	9.6	2.9	1.7	2.4	-1.1
1755	DALE G1	2.3	4.4	1.3	0.6	0.6	0.6
1756	DALE G2	497.2	932	279.6	163.4	217.2	-113.7

Comparing the results in Tables 4-10 and 4-11, the generation at buses 1754 and 1756 are identical from PSSE and PSLF. As for the generator on bus 1755 which has a difference between the upper VAr limit and the lower VAr limit less than *Minimum VAR limit band width* of 2MVArs in this case, the reactive power output of generator 1755 is automatically adjusted to the mid value between zero and the upper VAr limit in PSLF. The generators at buses 1754 and 1755 may be the small capacity auxiliary generators in the Dale power plant. The parameter, *Minimum VAR limit band width*, is used to prevent the small generators from trying to control the voltage of a strong system. But in some cases, a small capacity generator could also play an important role in the weak area under a stressed operating condition. Users need to determine which case applies to the study and then adjust the *Minimum VAR limit band width* carefully.

An inappropriate VAr limit control can result in generators bouncing on and off their VAr limit or even operating outside the VAr limit. PSLF and PowerWorld provide the control options for users to define the maximum number of times that a generator can operate outside its VAr limit range before the final solution is reached.

Newton's method cannot handle the generator reactive power limits very well. At the beginning of the solution, voltage mismatches requirements may not be satisfied due to that difficulty of allocating reactive power. It is reasonable to remove the VAr limits at the early stage of the solution and then apply the VAr limits after a few iterations. PSSE and PSLF can define at which iteration, VAr limits should be imposed to power flow solution. As the Newton method usually converges to the solution very fast, the VAr limit can be imposed on the third of fourth iteration.

4.5 Shunts and VAr Compensation

Switched shunts can change the admittance connected to PV buses and PQ buses, they can be either capacitive or inductive. Switched shunts at swing buses are usually locked. For the locked switched shunts, the admittance is held at a specified value during the solution. In all four software packages, up to 8 blocks of shunts can be combined as one static VAr system (SVS). Though the names of the control modes are different in each software package, there are mainly four types of control modes. They are fixed control mode, discrete control mode, continuous control mode and SVS control mode.

4.5.1 Fixed or Frozen Switched Shunt Control Mode

When the control mode is assigned to be fixed or frozen, the admittance will be locked at the specified values. Displayed reactive power generation values will follow the equation $Q_{shunt} = B_{step} * V^2$, where B_{step} is the shunt devices' susceptance.

When PSAT imports the raw file, despite the control mode being set as frozen, the default option moves the discrete shunts to the nearest steps which could be misleading in some cases. When PSAT imports the Texas system, the initial admittance of five switched shunts will be changed. They are the switched shunts at buses 528, 1224, 1228, 1363 and 1417, respectively. At the critical point, the power flow solution summary and the voltage profile comparison between PSSE and PSAT solutions are given in Table 4-12 and Figure 4-1, respectively. In Table 4-12, "$B_{Initial}$" represents the initial admittance in MVAr. "VAr" represents the actual reactive power produced by the switched shunts. Nominal represents the MVAr needed to hold the bus voltage at 1 per unit. Changes of shunts admittance in PSAT will result in unacceptably high voltages at some buses as shown in Figure 4-1.

Table 0-12 Frozen Shunt Control Mode

Bus	$B_{Initial}$	VAr	Nominal	Voltage
528	40	44.29	50	0.9412
1224	80	124.57	100	1.1161
1228	50	165.97	100	1.2883
1363	40	67.81	60	1.0631
1417	-10	0	0	1.0503

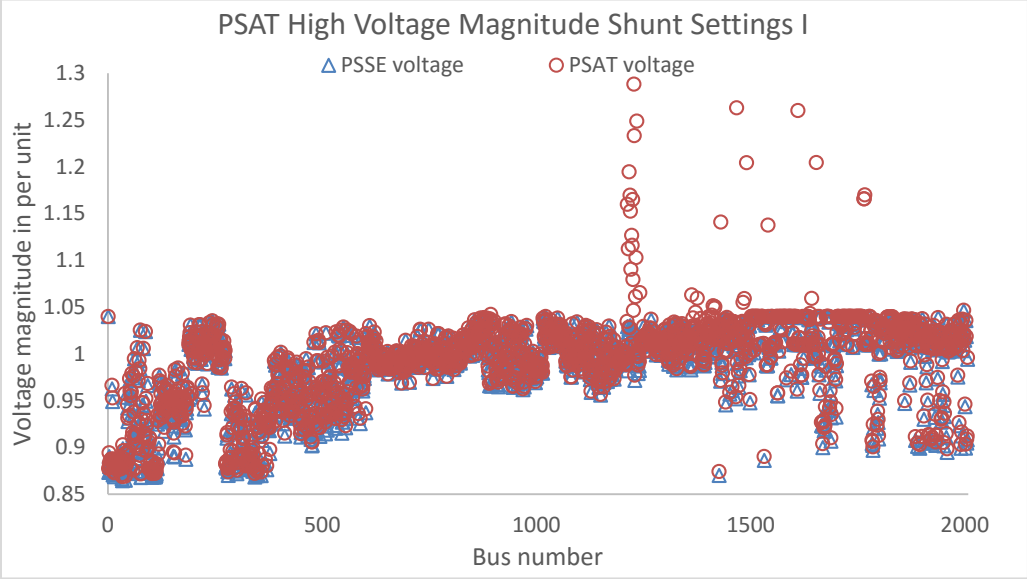

Figure 0-1 Frozen shunt control mode voltage profile

Bus 1224 and Bus 1228 have unrealistically high voltages which is not acceptable in normal power system operation. When PSAT changes the shunts admittance control mode, a notice will be given in the message window. Users can carefully adjust the shunt control settings based on the notice information. From Table 4-12 it is observed that the reactive power provided by the switched shunts satisfy the relation $Q_{shunt} = B_{step} * V^2$.

4.5.2 Continuous Switched Shunt Control Mode

When the control mode is assigned as continuous, the voltage of the controlled bus is held at the scheduled voltage as long as the admittance of the shunt devices are within their

limit. Switched shunt at its high limit means all reactors are switched off and all capacitors are switched on. Switched shunt at its low limit means all reactors are switched on and all capacitors are switched off.

If the switched shunts control mode is continuous, the high voltage issue no longer exists. At the critical point, the power flow solution summary and voltage profile comparison between PSSE and PSAT solutions are given in Table 4-13 and Figure 4-2, respectively.

Table 0-13 Continuous Shunt Control Mode

Bus	VAr	Nominal	Voltage
528	44.17	50.00	0.9399
1224	62.57	62.57	1
1228	44.90	44.90	1
1363	27.19	27.19	1
1417	-9.07	-9.08	0.9994

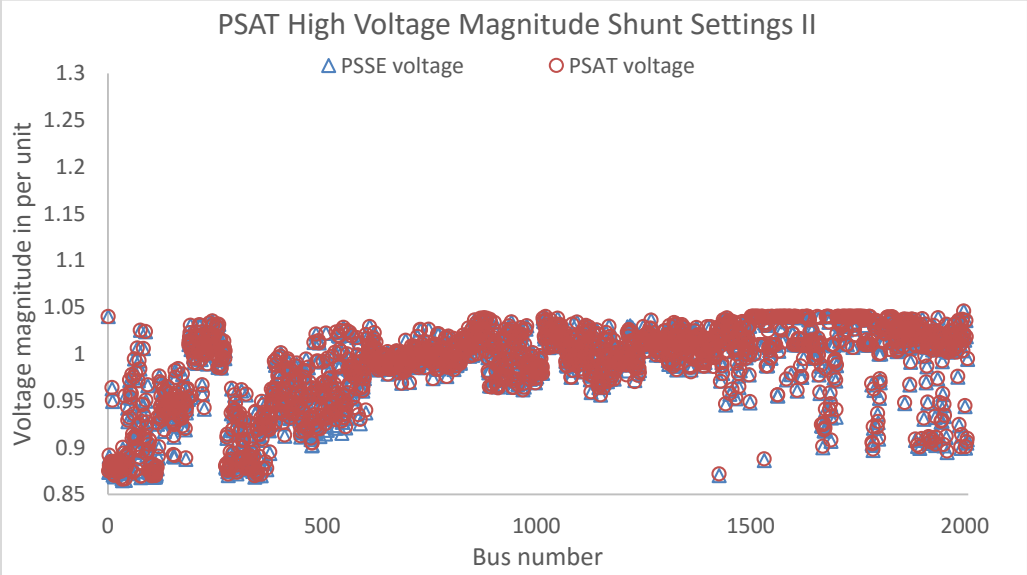

Figure 0-2 Continuous Shunt Control Mode Voltage Profile

As shown in Figure 4-2, once the control mode is switched from frozen to continuous, all voltages are within a normal range. The switched shunts try to hold the bus voltage at 1

per unit. At Bus 528 and Bus 1417, the bus voltages are close to but less than 1 per unit. That is because once the switched shunts reach their VAr limits, they can no longer hold the bus voltages at scheduled levels.

4.5.3 SVS Switched Shunt Control Mode

If the control mode is assigned as SVS, the adjustment results in continuous control. Thus, to apply the SVS control mode, the continuous shunts adjustment option should be checked in power flow programs. The bus voltage control will follow the specified droop characteristics. SVS has a droop characteristic and maintains the voltages close to but less than nominal voltages. The droop control characteristic is shown in Figure 4-3. When a SVS operates at its capacity limit, SVS becomes a simple capacitor, voltage control is no longer available.

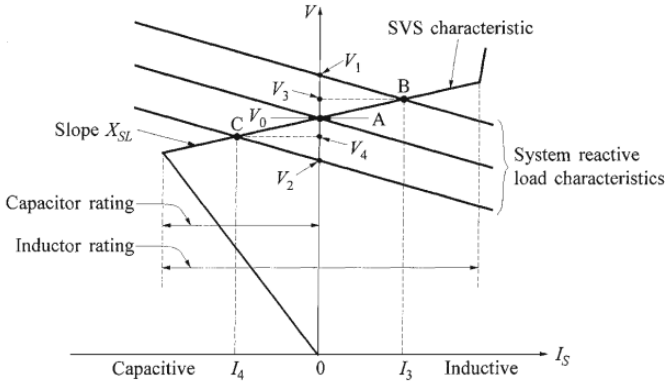

Figure 0-3 SVS Droop Control [4]

The negatively-sloped straight line passing through point A in the middle represents nominal operation condition load characteristics. If the load is increased, the voltage will drop from V_0 to V_2 without the SVS. When the SVS is applied, the voltage will drop from V_0 to V_4. Although the voltage is still lower than the original nominal value, V_4 is closer to nominal voltage compared to V_2. At the critical point, the power flow solution summary is

given in Table 4-14. As shown in the table, the bus voltage magnitudes are close to 1 per unit but less than 1 per unit for all buses except bus 528. That is because the switched shunt on bus 528 has reached its limit.

Table 0-14 SVS Shunt Control Mode

Bus	VAr	Nominal	Voltage
528	44.16	50.00	0.9398
1224	58.87	59.58	0.9940
1228	43.80	44.19	0.9956
1363	24.73	24.94	0.9958
1417	-10.31	-10.44	0.9935

4.5.4 Discrete Switched Shunt Control Mode

If the control mode is assigned as discrete, at K=1.032, the solution diverges. The non-converged solution is given in Table 4-15.

Table 0-15 Discrete Shunt Control Mode

Bus	VAr	Nominal	Voltage
528	44.77	50	0.9462
1224	0	0	1.7037
1228	0	0	3.7031
1363	0	0	0.9487
1417	-25.31	-30	0.9186

As the control mode is changed from continuous to discrete, there could be significant changes in bus voltages. These can cause convergence difficulty in the solution process. One way to overcome this issue is that the switched shunts could be treated as continuous mode control shunts before the solution converges. Once the solution satisfies the convergence tolerance, the discrete mode shunts could be set to the nearest steps and the case resolved. The solution process will continue with the discrete shunts fixed at the

admittance corresponding to the nearest step. This results in more iterations being required to reach the final solution.

Another possible reason for the discrete shunt control oscillating is that there may be some other devices or adjustment controlling the voltage or admittance of the discrete shunts at the same time. To prevent the oscillating adjustment of the discrete mode switched shunts, a maximum number of attempts on the switched shunts control can be applied. Once the maximum number of attempts is reached, the controls of the switched shunts are no longer available.

4.5.5 VAr Compensation

From the previous study, bus 34 has the lowest voltage magnitude in the system. This bus also participates in mode 1 of the critical case modal analysis. No generator exists close to this bus. The closest generator is about six buses away. Hence, a FACTs device is installed at bus 34 to provide VAr compensation. The maximum reactive power production is set to be 300MVAr for this device and the target voltage magnitude is 1.0 per unit. Table 4-16 summarizes the reactive support needed to maintain the voltage magnitude at 1 per unit by different software packages. The results in this table show that all four packages show the same amount of required VAr compensation at bus 34.

Table 0-16 VAr Compensation VAr Production

Software	VAr needed
PSSE	267.8 MVAr
PSLF	267.9 MVAr
PSAT	267.3 MVAr
PowerWorld	267.8 MVAr

After the VAr compensation device is added at bus 34, there is a significant improvement in system voltage profile. The voltage magnitude comparison before and after VAr compensation for the four software packages are shown in Figure 4-4 to Figure 4-7.

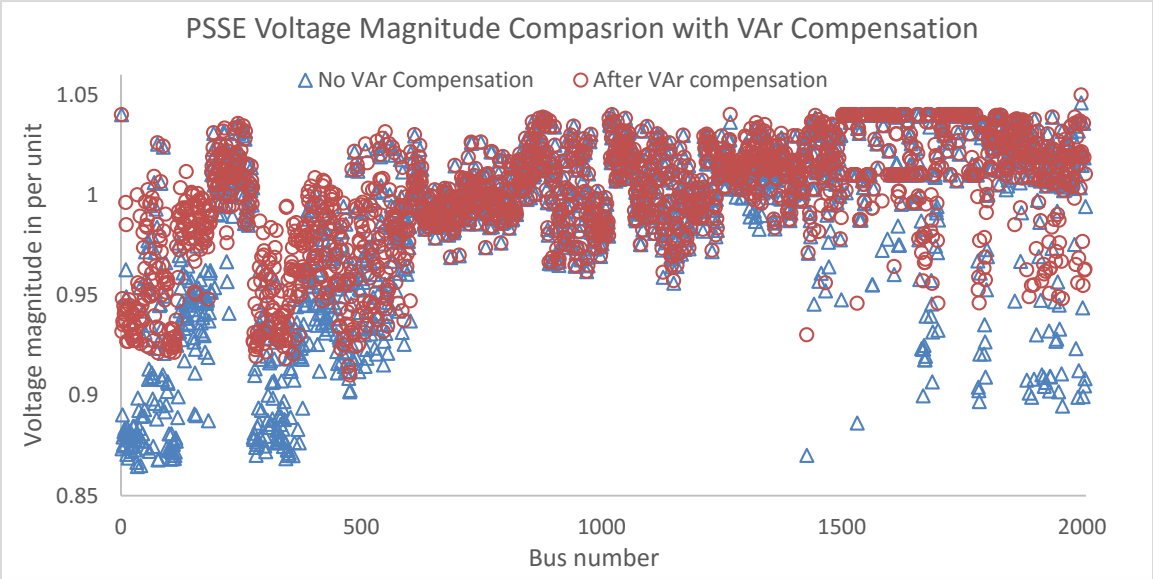

Figure 0-4 PSSE Voltage Profile with VAr Compensation

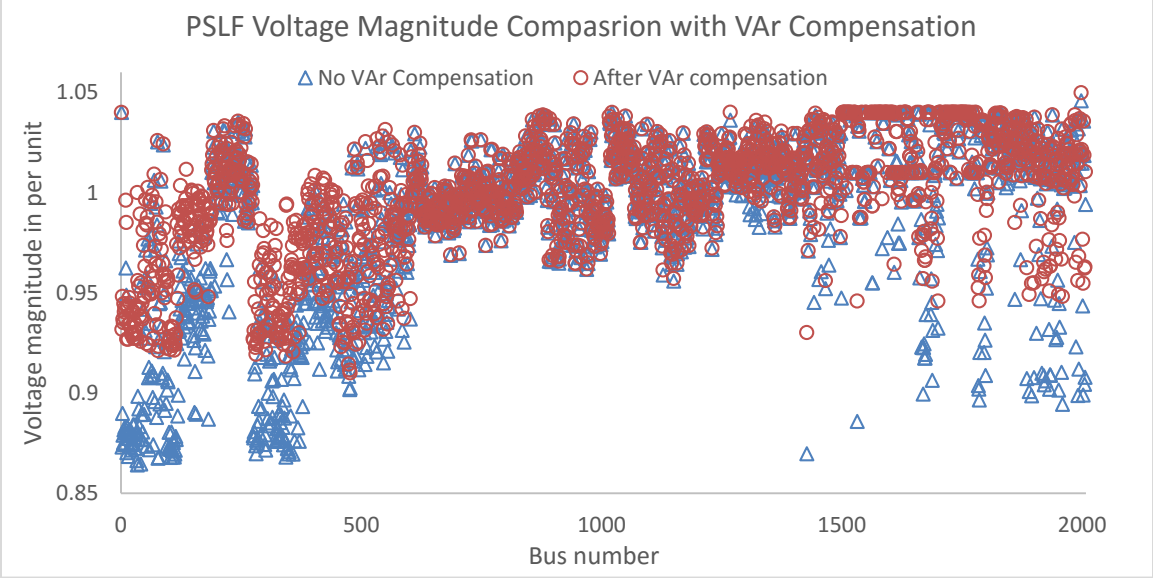

Figure 0-5 PSLF Voltage Profile with VAr Compensation

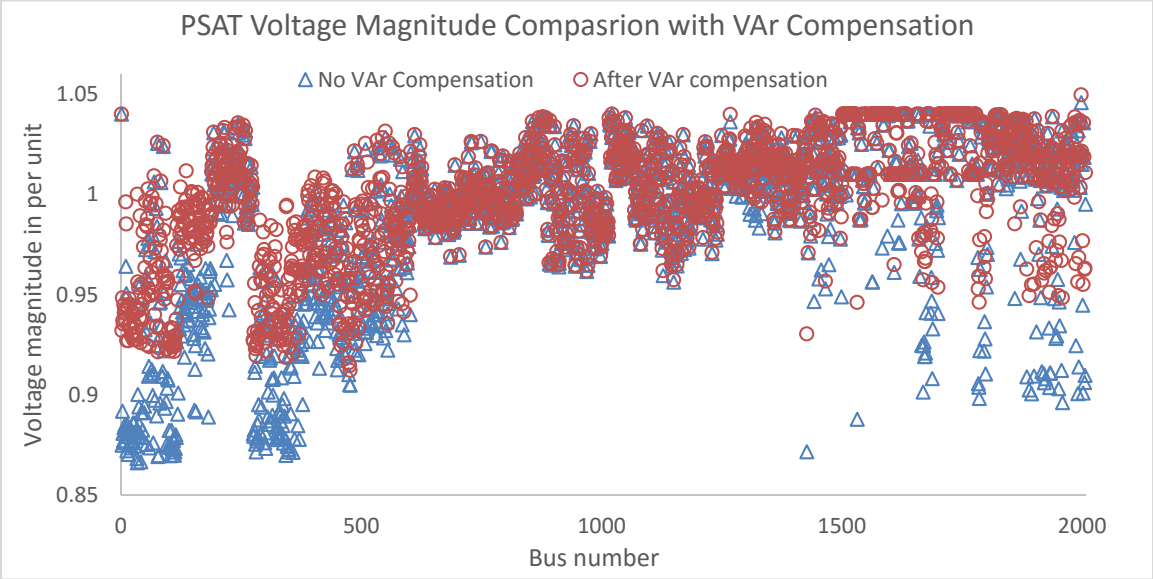

Figure 0-6 PSAT Voltage Profile with VAr Compensation

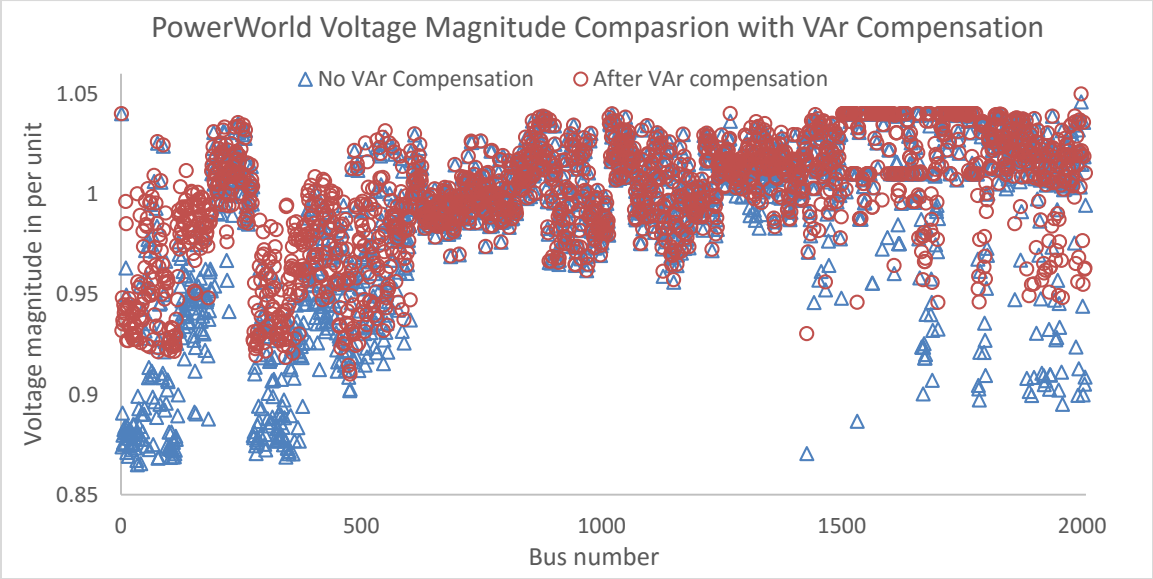

Figure 0-7
PowerWorld Voltage Profile with VAr Compensation

The modal analysis results for K=1.032 case, before and after VAr compensation are given in Table 4-17 and Table 4-18.

Table 0-17 Modal Analysis at *K*=1.032 without VAr Compensation

No.	Bus	Gen	Part.Fac.	Voltage
1	1668	QL	1.00000	0.9246
2	1532	QL	0.95166	0.8878
3	6		0.80054	0.8836
4	31		0.79661	0.8814
5	182		0.79347	0.8889
6	350		0.79236	0.8727
7	346		0.78725	0.8745
8	34		0.78683	0.8661
9	156		0.78599	0.8915
10	153		0.78055	0.8923
11	154		0.77822	0.9127
12	1667	QL	0.77472	0.9246
13	347		0.76887	0.8742
14	36		0.76271	0.8791
15	18		0.76069	0.8805
16	181		0.75929	0.9204
17	1670	QL	0.75907	0.9246
18	41		0.75616	0.8666
19	119		0.75256	0.9009
20	33		0.75143	0.8682

Table 4-17 above only shows the buses with the largest 20 bus participation factors for the most critical mode 1 without VAr compensation. In fact, there are more than 100 generators having a large bus participation factors in mode 1. Thus, this operating point can be viewed as a voltage collapse critical point affecting a significant portion of the system. The smallest eigenvalue is 0.036708 for the critical case without VAr compensation. Bus 34 has the lowest voltage magnitude among all mode 1 buses. By adding a VAr compensation device to bus 34, the smallest eigenvalue for the *K*=1.032 case becomes 0.146453. After the VAr compensation device is added, all the buses in mode 1 to

mode 9 are generator buses with acceptable voltage magnitudes. The bus participation factors for those load buses which have large bus participation factors in the original mode 1 are less than 0.001 now. The voltage stability is enhanced system wide by adding this VAr compensation device.

Table 0-18 Modal Analysis at K=1.032 with VAr Compensation

Mode	Eigen	No.	Bus	Gen	Part.Fac.	Voltage
1	0.146453	1	1660	QL	1.00000	0.9781
2	0.163553	1	1509	QL	1.00000	1.0009
3	0.174013	1	1710	QL	1.00000	1.0328
4	0.185574	1	1569	QL	1.00000	1.0277
		2	1533	QL	0.18246	1.0332
		3	1535	QL	0.00103	1.0332
		4	1534	QL	0.00103	1.0332
5	0.188326	1	1533	QL	1.00000	1.0332
		2	1569	QL	0.18521	1.0277
		3	1535	QL	0.00155	1.0332
		4	1534	QL	0.00155	1.0332
6	0.191428	1	1668	QL	1.00000	0.9791
7	0.264016	1	1623	QL	1.00000	1.0100
8	0.272429	1	1540	QL	1.00000	0.9875
		2	1539	QL	1.00000	0.9875
		3	1537	QL	0.02532	0.9875
		4	1538	QL	0.00563	0.9875
9	0.279794	1	1539	QL	1.00000	0.9875
		2	1540	QL	1.00000	0.9875

Table 4-19 shows the smallest five eigenvalues for both cases. The smallest eigenvalue has increased significantly with VAr compensation while eigenvalue of other modes also increased moderately.

Table 0-19 Eigenvalue Comparison for the *K*=1.032 Case without and with Compensation

Eigenvalue	No Compensation	With VAr Compensation
Smallest	0.036708	0.146453
2nd	0.146318	0.163553
3rd	0.163196	0.174013
4th	0.17207	0.185574
5th	0.173968	0.188326

Table 4-20 gives the new critical *K* using the four software packages after adding VAr compensation at bus 34.

Table 0-20 Critical Value with VAr Compensation

Critical *K*	PSSE	PSLF	PSAT	PowerWorld
No Compensation	1.032	1.032	1.033	1.032
With Compensation	1.052	1.053	1.052	1.051
VAr Support on bus 34	286.9	300	287.75	272.75

The VAr compensation on Bus 34 can increase the critical loading level. An increase of 0.02 in the critical value of *K* corresponds to a load increase of 995.51MW in the whole system.

In conclusion, modal analysis gives a good indication of the buses in the system which are weak buses. The bus participation factors can determine whether the voltage instability is localized or non-localized. Once the weak areas and weak buses are found, reactive power compensation devices can be added at those buses to improve the static voltage stability.

4.6 Area Interchange

To enable area interchange adjustment, users need to check the area interchange option in PSSE, PSLF and PSAT. In PowerWorld, automatic generation control must be applied to implement the area interchange control. There are five different area interchange modes in PowerWorld. They are *Participation Factor Control*, *Economic Dispatch Control*, *Area Slack Bus Control*, *Injection Group Area Slack Control* and *Optimal Power Flow*. *Economic Dispatch Control* and *Optimal Power Flow* require realistic generation cost functions to implement area interchange. *Participation Factor Control* and *Injection Group Area Slack Control* allow the users to define the generator output adjustment. For example, generator output changes can be set in proportion to the generator capacity or in proportion to the generator's active power output margin. There are also other methods to adjust generator output in PowerWorld. More details can be found in [20]. When *Area Slack Bus Control* is applied, only the area slack buses participate in area interchange control. In this study, the area slack bus control method and the Texas system critical case, where K=1.032, are tested in all four software packages.

After the area interchange control is enabled, users need to define the area slack buses. Each area can have one specified area slack bus. The area slack bus is not mandatory, since it is not necessary for all areas to participate in the area interchange. Each slack bus should have at least one in-service generator connected to it. For this study, the generator which has the largest MW capacity in the area is selected as the area slack bus. If the largest generator in an area is already at its limit, the second largest generator is selected as the area slack and so on. The selected area slack buses are shown in Table 4-21.

Table 0-21 Area Slack Bus Selection

Area	1	2	3	4	5	6	7	8
Slack Bus	1	1693	1682	1730	1705	1554	1593	1735

The adjustments for the area slack buses usually are continuous, unless the area net interchange mismatches are larger than the tolerance. If the area interchange tolerance is too small, it could result in non-convergence problems. For a large power system with more than 1000MW net interchange, the tolerance can be set as10MW. The desired net interchanges need to be specified for each area. A positive desired value represents an area exporting the active power to other areas and a negative desired value represents an area importing active power from other areas.

Table 4-22 and Table 4-23 provide the PSSE actual and desired power export results with the area interchange control off and on, respectively. Table 4-24 gives the PSSE slack bus generation under both cases.

Table 0-22 PSSE Area Interchange off

Area	Exported *P* in MW	Desired *P* in MW	Export *Q* in MVAr
1	-3562.3	-3500	-1316
2	2051.8	2000	402.7
3	2575.2	2500	759.3
4	-1040.7	-1000	-278.3
5	2050.8	2000	857.9
6	2063.1	2000	-458.7
7	-5683.2	-5500	-377.4
8	1545.3	1500	410.4

Table 0-23 PSSE Area Interchange on

Area	Exported *P* in MW	Desired *P* in MW	Export *Q* in MVAr
1	-3500	-3500	-1146.3
2	2000	2000	320.5
3	2500	2500	714.3
4	-1000	-1000	-270.7
5	2000	2000	812.5
6	2000	2000	-454.4
7	-5500	-5500	-386.2
8	1500	1500	410.2

Table 0-24 PSSE Area Slacks Generation

Area	1	2	3	4	5	6	7	8
P_{AI_off} MW	2365.4	637.8	878.6	901.7	351.3	463.7	1484.5	1512.6
Q_{AI_off} MVAr	1481.9	219	270.8	15.2	171.2	14.6	92.9	35.1
P_{AI_on} MW	2413.3	583.7	799.9	939.6	295.8	399.1	1667.8	1467
Q_{AI_on} MVAr	1371.2	184.8	239.1	12.5	162.8	11.1	109.8	32.5

Table 4-25 and Table 4-26 give the PSLF actual and desired power export results with area interchange control off and on, respectively. Table 4-27 gives the PSLF slack bus generation under both cases.

Table 0-25 PSLF Area Interchange off

Area	Exported *P* in MW	Desired *P* in MW	Export *Q* in MVAr
1	-3562.2	-3500	-1320.1
2	2051.8	2000	404.7
3	2575.2	2500	760.3
4	-1040.7	-1000	-278.3
5	2050.8	2000	859
6	2063.1	2000	-458.6
7	-5683.2	-5500	-377.4
8	1545.3	1500	410.5

Table 0-26 PSLF Area Interchange on

Area	Exported *P* in MW	Desired *P* in MW	Export *Q* in MVAr
1	-3499.8	-3500	-1148.2
2	1999.9	2000	321.6
3	2499.6	2500	714.9
4	-1000.1	-1000	-270.7
5	2000.3	2000	812.9
6	2000	2000	-454.4
7	-5500	-5500	-386.3
8	1500.2	1500	410.2

Table 0-27 PSLF Area Slacks Generation

Area	1	2	3	4	5	6	7	8
P_{AI_off} MW	2365.8	637.8	878.6	901.7	351.3	463.7	1484.5	1512.6
Q_{AI_off} MVAr	1485.1	220.3	271.4	15.2	171.3	14.7	92.9	35.1
P_{AI_on} MW	2413.6	583.6	799.5	939.5	296.1	399	1667.8	1467.2
Q_{AI_on} MVAr	1372.8	185.7	239.4	12.5	162.8	11.1	109.8	32.5

Table 4-28 and Table 4-29 give the PSAT actual and desired power export results with area interchange control off and on, respectively. Table 4-30 gives the PSAT slack bus generation under both cases.

Table 0-28 PSAT Area Interchange off

Area	Exported *P* in MW	Desired *P* in MW	Export *Q* in MVAr
1	-3562.9	-3500	-1288
2	2052.01	2000	393.34
3	2575.28	2500	753.59
4	-1040.7	-1000	-278.06
5	2050.91	2000	837.78
6	2063.45	2000	-453.37
7	-5683.2	-5500	-377.62
8	1545.19	1500	412.35

Table 0-29 PSAT Area Interchange on

Area	Exported *P* in MW	Desired *P* in MW	Export *Q* in MVAr
1	-3507.1	-3500	-1128.6
2	2000.07	2000	316.37
3	2499.97	2500	710.28
4	-999.99	-1000	-271.06
5	2006.85	2000	796.06
6	2000.01	2000	-448.94
7	-5499.9	-5500	-386.18
8	1500.25	1500	412.12

Table 0-30 PSAT Area Slacks Generation

Area	1	2	3	4	5	6	7	8
P_{AI_off} MW	2363.45	637.84	878.55	901.65	351.3	463.7	1484.46	1512.58
Q_{AI_off} MVAr	1466.77	215.57	266.99	15.22	171.99	15.97	92.82	36.5
P_{AI_on} MW	2405.45	583.68	799.79	939.71	302.4	398.72	1667.76	1467.39
Q_{AI_on} MVAr	1362.8	183.3	236.48	12.62	163.33	12.39	109.74	33.92

Table 4-31 and Table 4-32 give the PowerWorld actual and desired power export results with area interchange control off and on, respectively. Table 4-33 gives the PowerWorld slack bus generation under both cases.

Table 0-31 PowerWorld Area Interchange off

Area	Exported *P* in MW	Desired *P* in MW	Export *Q* in MVAr
1	-3562.49	-3500	NA
2	2051.88	2000	NA
3	2575.26	2500	NA
4	-1040.73	-1000	NA
5	2050.85	2000	NA
6	2063.13	2000	NA
7	-5683.24	-5500	NA
8	1545.3	1500	NA

Table 0-32 PowerWorld Area Interchange on

Area	Exported *P* in MW	Desired *P* in MW	Export *Q* in MVAr
1	-3500.19	-3500	NA
2	2000.12	2000	NA
3	2499.93	2500	NA
4	-999.94	-1000	NA
5	1999.98	2000	NA
6	1999.98	2000	NA
7	-5500	-5500	NA
8	1500.25	1500	NA

Table 0-33 PowerWorld Area Slacks Generation

Area	1	2	3	4	5	6	7	8
P_{AI_off} MW	2364.82	637.84	878.55	901.65	351.3	463.7	1484.54	1512.58
Q_{AI_off} MVAr	1477.91	218.09	269.98	15.2	171.19	14.64	92.85	35.07
P_{AI_on} MW	2413.11	583.78	799.84	939.68	295.75	399.07	1667.78	1467.27
Q_{AI_on} MVAr	1371.18	184.84	239.08	12.53	162.83	11.15	109.76	32.49

Results from all four software packages are very similar. The voltage magnitude comparisons are given in Figure 4-8 to Figure 4-11.

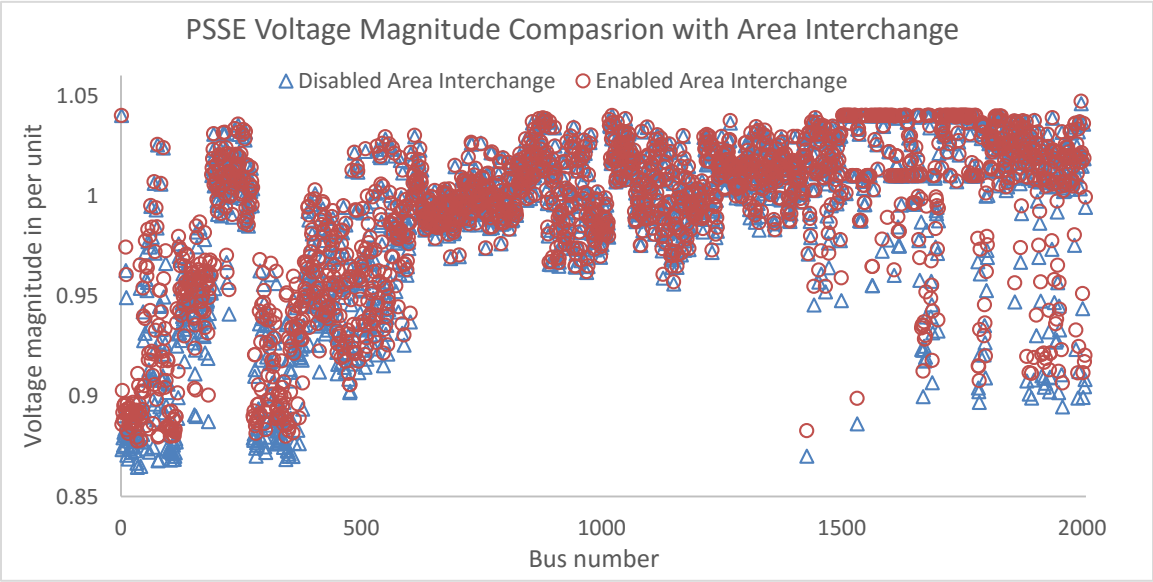

Figure 0-8 PSSE Voltage Magnitude with Area Interchange

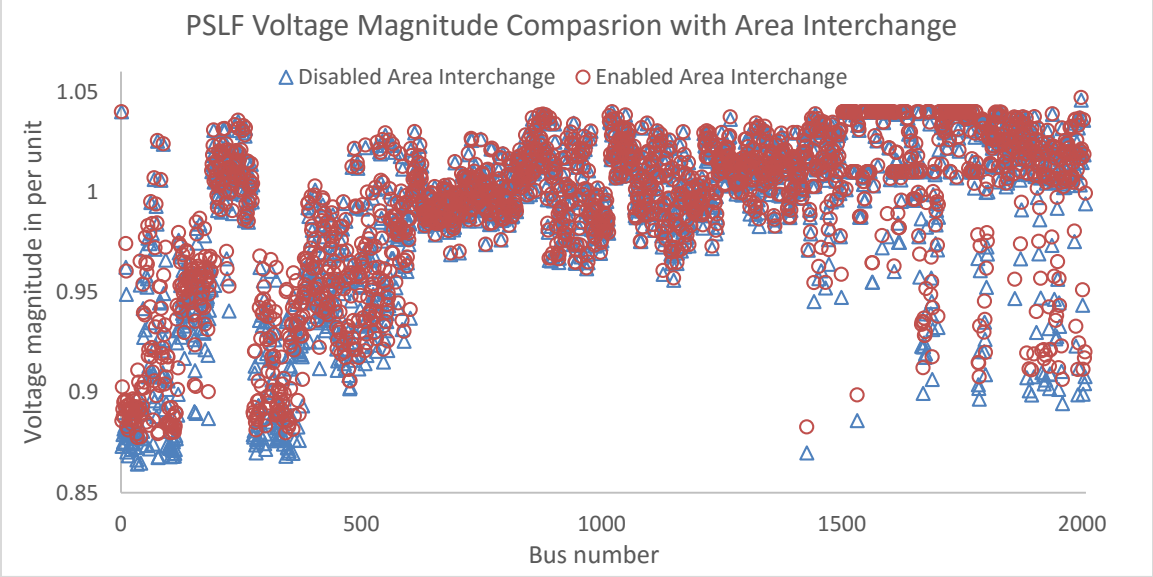

Figure 0-9 PSLF Voltage Magnitude with Area Interchange

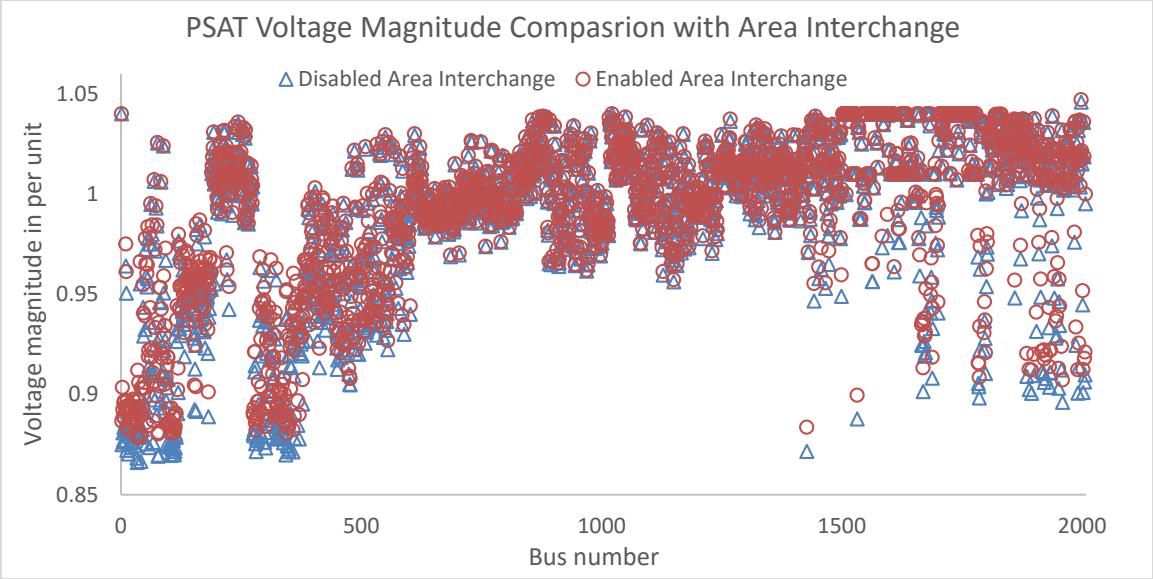

Figure 0-10 PSAT Voltage Magnitude with Area Interchange

As shown in the voltage magnitude comparison figures, with area interchange control applied, the voltage magnitude profile is improved in this case. Modal analysis results for mode 1 for both cases are given in Table 4-34 and Table 4-35.

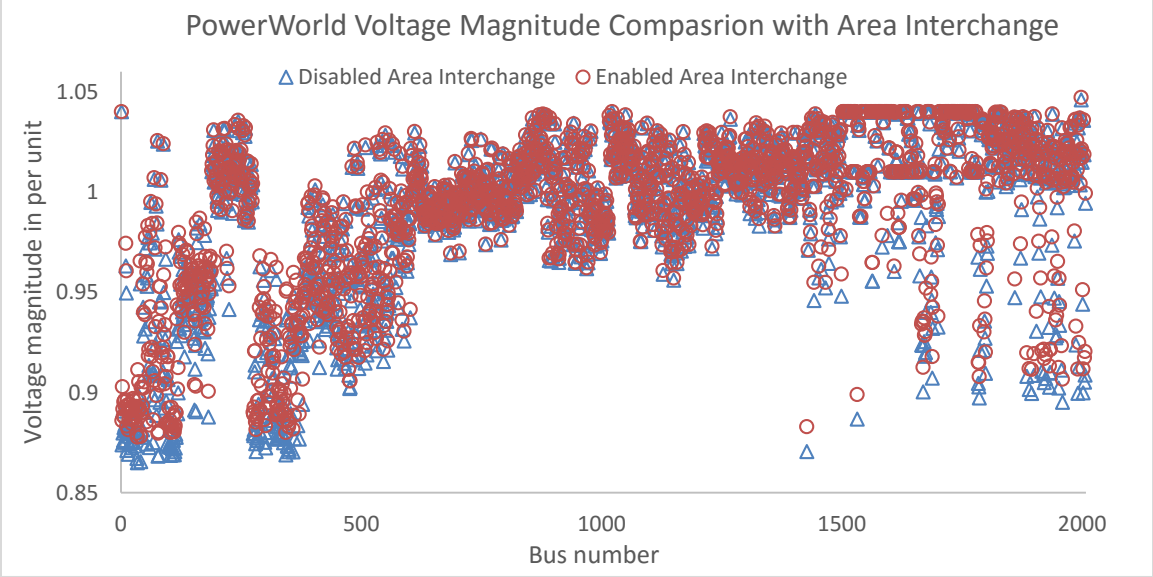

Figure 0-11 PowerWorld Voltage Magnitude with Area Interchange

Table 0-34 Modal Analysis without Area Interchange

No.	Bus	Gen	Part.Fac.	Voltage
1	1668	QL	1	0.9246
2	1532	QL	0.95166	0.8878
3	6		0.80054	0.8836
4	31		0.79661	0.8814
5	182		0.79347	0.8889
6	350		0.79236	0.8727
7	346		0.78725	0.8745
8	34		0.78683	0.8661
9	156		0.78599	0.8915
10	153		0.78055	0.8923
11	154		0.77822	0.9127
12	1667	QL	0.77472	0.9246
13	347		0.76887	0.8742
14	36		0.76271	0.8791
15	18		0.76069	0.8805
16	181		0.75929	0.9204
17	1670	QL	0.75907	0.9246
18	41		0.75616	0.8666
19	119		0.75256	0.9009
20	33		0.75143	0.8682

Table 0-35 Modal Analysis with Area Interchange

No.	Bus	Gen	Part.Fac.	Voltage
1	1668	QL	1	0.9361
2	1532	QL	0.80778	0.8996
3	1667	QL	0.62225	0.9361
4	1670	QL	0.60035	0.9361
5	154		0.58453	0.9246
6	181		0.57145	0.9322
7	155		0.56124	0.9362
8	6		0.55883	0.896
9	182		0.55534	0.9012
10	175		0.55523	0.9349
11	31		0.55494	0.8937
12	156		0.54998	0.9038
13	350		0.54518	0.8852
14	153		0.54498	0.9046
15	346		0.54063	0.887
16	169		0.54048	0.9437
17	34		0.5395	0.8784
18	1669	QL	0.53594	0.9132
19	126		0.53446	0.841
20	173		0.53345	0.9429

When the area interchange is disabled the smallest eigenvalue is 0.036708. When the area interchange is enabled, the smallest eigenvalue is 0.061304. Modal analysis results also show that in this case, static voltage stability is enhanced by applying area interchange. The case study in next chapter will show that this is not always true. The relationship between the area interchange control and static voltage stability is case dependent. It usually depends on the power transfer path and the location of the generation and load pockets.

CHAPTER 5

TEXAS SYSEM AREA INTERCHANGE CASE STUDY

5.1 Introduction

According to the ERCOT 2012 Long-Term System Assessment (LTSA) report [34], the Panhandle region will provide a significant amount of renewable energy in the near future. The Panhandle region is located in area 2 (North). Area 7 (Coast) is an important load center, which contains the Houston area. An additional power transfer from area 2 to area 7 could result in voltage stability issues, since the Panhandle area lacks a significant reactive power source. Table 5-1 shows the base case generation and load for area 2 and area 7.

Table 0-1 Base Case Information

	Area 2 (North)	Area 7 (Coast)
P_{Gen} MW	3008.36	9085.066
P_{Total} MW	8440.1	17106.5
Q_{Gen} MVAr	-369.761	2274.655
Q_{Total} MVAr	2004.671	4223.581
P_{Load} MW	930.471	14420.651
Q_{Load} MVAr	265.182	4109.881

In this study, both the real and reactive power load in area 7 is uniformly scaled by the area scaling factor *K*. Generation in area 2 is scaled up to meet the increase in demand. If the percentage load in area 7 is increased by $(K-1)*100\%$, the generation in area 2 is increased by $(K*\frac{14420.65}{3008.36}*100\%)$. Where 14420.65MW is the base case area 7 active power load and 3008.36MW is the base case area 2 active power generation.

5.2 Area Interchange

The critical *K* found by all four software packages are identical which is 1.10. The results presented in this study are all from PSAT. Table 5-2 and Table 5-3 give the PSAT actual and desired power export with area interchange control off and on, respectively. Table 5-4 gives the PSAT slack bus generations for both cases. In Table 5-4, P_{AI_off} and Q_{AI_off} represent the active power and reactive power generated by the slack generators when the area interchange control is disabled, respectively. P_{AI_on} and Q_{AI_on} represent the active power and reactive power generated by the slack generators when the area interchange control is enabled, respectively.

Table 0-2 PSAT Area Interchange Control off

Area	Exported *P* in MW	Desired *P* in MW	Export *Q* in MVAr
1	-3204.5	-3500	-1467
2	3374.35	3442	232.65
3	2450.97	2500	1156.31
4	-1029.5	-1000	-184.43
5	1922.03	2000	767.61
6	1989.9	2000	-384.73
7	-7001.1	-6942	-567.29
8	1497.94	1500	446.91

Table 0-3 PSAT Area Interchange Control on

Area	Exported *P* in MW	Desired *P* in MW	Export *Q* in MVAr
1	-3498.8	-3500	-1453.2
2	3441.87	3442	267.16
3	2499.66	2500	1116.4
4	-999.76	-1000	-202.02
5	1999.17	2000	791.14
6	1999.87	2000	-394.57
7	-6942	-6942	-563.83
8	1500.04	1500	438.99

Table 0-4 PSAT Area Slacks Generations

Area	1	2	3	4	5	6	7	8
P_{AI_off} MW	2604.71	914.33	851.31	873.7	340.41	449.32	1438.51	1465.68
Q_{AI_off} MVAr	1446.78	266.02	464.38	52.54	234.68	26.11	177.69	37.76
P_{AI_on} MW	2303.06	984.45	894.26	903.11	409.56	457.85	1496.22	1467.72
Q_{AI_on} MVAr	1427.93	292.93	428.92	53.44	234.86	24.22	180.35	33.7

If the desired export values are not changed, the area slack generator outputs are as given in Table 5-5.

Table 0-5 PSAT Area Slacks Generations with Export Values Unchanged

Area	1	2	3	4	5	6	7	8
P MW	2185.93	-467.11	851.61	877.1	352.06	448.16	2948.13	1465.95
Q MVAr	892.02	171.46	149.91	27.14	140.92	9.34	437.13	3.81

As the area interchange is adjusted using the area slack control mode, all the net interchange mismatches are picked up by the area slack generators. If the desired area export values are not modified and stay the same as the base case values, the area 2 slack generator will have a negative active power output due to over-generation in area 2, which is impractical. Therefore, when the area interchange option is invoked, the desired export values should be chosen appropriately to reach an acceptable steady state operating condition.

The net power transfer between areas of the base case, critical case with area interchange control off and critical case with area interchange control on are shown in Table 5-6, Table 5-7 and Table 5-8, respectively.

Table 0-6 Base Case Area Net Power Transfer

To Area / From Area	1	2	3	4	5	6	7	8
1		*P* -1780.49MW *Q* 100.54MVAr	*P* 526.08MW *Q* -269.90MVAr	*P* -245.76MW *Q* 9.35MVAr	*P* -2000.02MW *Q* -162.13MVAr			
2	*P* 1780.49MW *Q* -100.54MVAr		*P* 35.89MW *Q* -0.61MVAr		*P* 324.28MW *Q* -73.67MVAr	*P* -140.55MW *Q* 25.62MVAr		
3	*P* -526.08MW *Q* 269.90MVAr	*P* -35.89MW *Q* 0.61MVAr		*P* 66.76MW *Q* -53.40MVAr			*P* 2995.25MW *Q* 303.40MVAr	
4	*P* 245.76MW *Q* -9.35MVAr		*P* -66.76MW *Q* 53.40MVAr		*P* -2107.34MW *Q* 39.71MVAr		*P* 1900.89MW *Q* -9.83MVAr	*P* -972.60MW *Q* -324.15MVAr
5	*P* 2000.02MW *Q* 162.13MVAr	*P* -324.28MW *Q* 73.67MVAr		*P* 2107.34MW *Q* -39.71MVAr		*P* -1859.48MW *Q* 434.14MVAr		*P* 76.46MW *Q* -19.38MVAr
6		*P* 140.55MW *Q* -25.62MVAr			*P* 1859.48MW *Q* -434.14MVAr			
7			*P* -2999.25MW *Q* -303.40MVAr	*P* -1900.89MW *Q* 9.83MVAr				*P* -603.85MW *Q* -20.47MVAr
8				*P* 972.60MW *Q* 324.15MVAr	*P* -76.46MW *Q* 19.38MVAr		*P* 603.85MW *Q* 20.47MVAr	

Table 0-7 Critical Case with Area Interchange Control off Area Net Power Transfer

To Area / From Area	1	2	3	4	5	6	7	8
1		*P* -2640.69MW *Q* -267.63MVAr	*P* 1554.15MW *Q* -716.53MVAr	*P* -243.40MW *Q* -3.25MVAr	*P* -1874.5MW *Q* -479.62MVAr			
2	*P* 2640.69MW *Q* 267.63MVAr		*P* 42.38MW *Q* 2.88MVAr		*P* 652.52MW *Q* -30.16MVAr	*P* 38.76MW *Q* -7.71MVAr		
3	*P* -1554.15MW *Q* 716.53MVAr	*P* -42.38MW *Q* -2.88MVAr		*P* 89.81MW *Q* -63.14MVAr			*P* 3957.68MW *Q* 505.80MVAr	
4	*P* 243.40MW *Q* 3.25MVAr		*P* -89.81MW *Q* 63.14MVAr		*P* -2646.94MW *Q* 109.09MVAr		*P* 2318.75MW *Q* 19.98MVAr	*P* -854.91MW *Q* -379.89MVAr
5	*P* 1874.59MW *Q* 479.62MVAr	*P* -652.52MW *Q* 30.16MVAr		*P* 2646.94MW *Q* -109.09MVAr		*P* -2028.66MW *Q* 392.43MVAr		*P* 81.68MW *Q* -25.51MVAr
6		*P* -38.76MW *Q* 7.71MVAr			*P* 2028.66MW *Q* -392.43MVAr			
7			*P* -3957.68MW *Q* -505.80MVAr	*P* -2318.75MW *Q* -19.98MVAr				*P* -724.71MW *Q* -41.51MVAr
8				*P* 854.91MW *Q* 379.89MVAr	*P* -81.68MW *Q* 25.51MVAr		*P* 724.71MW *Q* 41.51MVAr	

Table 0-8 Critical Case with Area Interchange Control on Area Net Power Transfer

To Area / From Area	1	2	3	4	5	6	7	8
1		*P* -2720.4MW *Q* -299.92MVAr	*P* 1417.58MW *Q* -673.76MVAr	*P* -244.56MW *Q* -1.55MVAr	*P* -1951.4MW *Q* -478.03MVAr			
2	*P* 2720.40MW *Q* 299.92MVAr		*P* 42.52MW *Q* 3.26MVAr		*P* 648.18MW *Q* -28.06MVAr	*P* 30.77MW *Q* -7.97MVAr		
3	*P* -1417.5MW *Q* 673.76MVAr	*P* -42.52MW *Q* -3.26MVAr		*P* 74.04MW *Q* -57.03MVAr			*P* 3885.72MW *Q* 502.93MVAr	
4	*P* 244.56MW *Q* 1.55MVAr		*P* -74.04MW *Q* 57.03MVAr		*P* -2645.3MW *Q* 92.59MVAr		*P* 2329.09MW *Q* 18.76MVAr	*P* -854.06MW *Q* -371.96MVAr
5	*P* 1951.42MW *Q* 478.03MVAr	*P* -648.18MW *Q* 28.06MVAr		*P* 2645.31MW *Q* -92.59MVAr		*P* -2030.6MW *Q* 402.53MVAr		*P* 81.26MW *Q* -24.89MVAr
6		*P* -30.77MW *Q* 7.97MVAr			*P* 2030.64MW *Q* -402.53MVAr			
7			*P* -3885.7MW *Q* -502.93MVAr	*P* -2329.0MW *Q* -18.76MVAr				*P* -727.24MW *Q* -42.14MVAr
8				*P* 972.60MW *Q* 324.15MVAr	*P* -76.46MW *Q* 19.38MVAr		*P* 603.85MW *Q* 20.47MVAr	

5.2.1 Area Interchange On

Table 5-9 shows the power transfer differences between the base case and the critical case with area interchange control on. Both absolute values and percentages of the differences between the two cases are given. The bold values indicate that the power transfer in the critical case increased compared to the base case. The unbolded values indicate that the power transfer in the critical case decreased compared to the base case. The summation of column 7 of Table 5-9 is $(890.47 + 428.25 + 123.4) = 1442.12$ MW. And the amount of load increase in area 7 is 1442.65 MW, which verifies that the load increase in area 7 is picked up by the other generators in the other areas. The summation of the row 3 of Table 5-9 is $(939.91 + 6.63 + 323.9 + 171.32) = 1441.76$ MW, which indicates that all the additional generation in area 2 is exported to balance the load increase in area 7.

Table 0-9 Power Transfer Difference I

To Area / From Area	1	2	3	4	5	6	7	8
1			**891.5MW 169.5%**					
2	**939.91MW 52.8%**		**6.63MW 18.5%**		**323.9MW 99.9%**	**171.32MW 121.8%**		
3				**7.28MW 10.9%**			**890.47MW 29.7%**	
4	-1.2MW -0.5%						**428.25MW 22.5%**	
5	-48.6MW -2.4%			**537.97MW 25.5%**				**4.8MW 6.3%**
6					**171.16MW 9.2%**			
7								
8				-118.54MW -12.2%			**123.4MW 20.4%**	

There is no inter-tie directly connecting area 7 to area 2. In order to find out the power transfer paths, Figure 5-1 and Figure 5-2 depict the path of the area interchanged in the system. Area numbers and corresponding area names are given in Table 5-10. Figure 5-1

shows the power transfer paths in the base case. Figure 5-2 shows the power transfer differences between the base case and the critical case with area interchange. In Figure 5-2, the red arrows represent that the net area interchange in the critical case is increased compared to the base case. The green arrows represent that the net area interchange in the critical case decreases compared to the base case.

Table 0-10 Area Numbers and Area Names

Area number	Area name
1	North Central
2	North
3	East
4	South Central
5	West
6	Far West
7	Coast
8	Southern

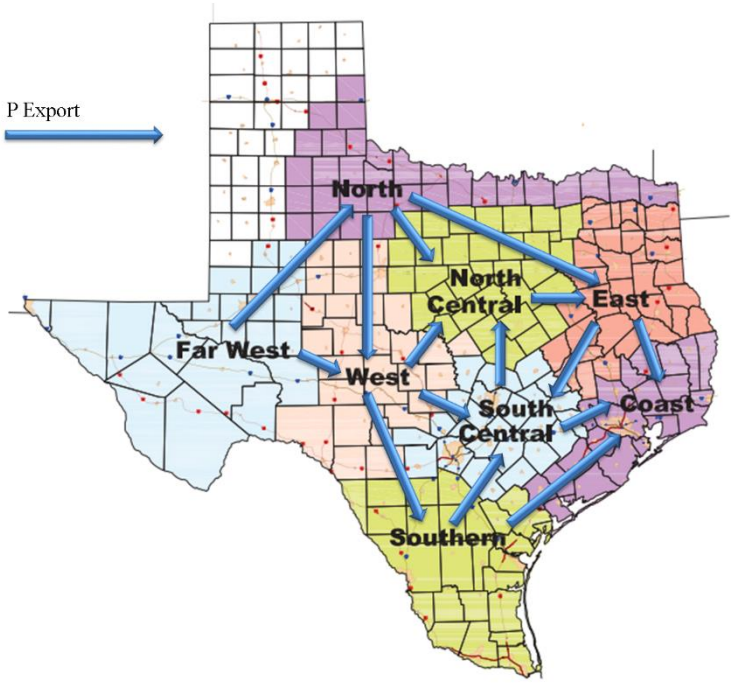

Figure 0-1 Base Case Power Transfer [35]

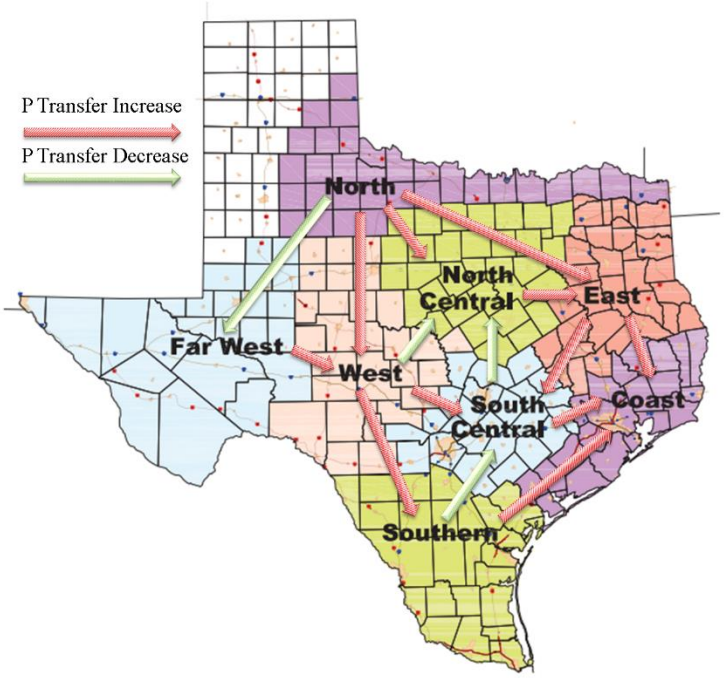

Figure 0-2 Power Transfer Difference

As shown in Figure 5-1 and Figure 5-2, the main power transfer path from area 2 to area 7 is North (2) → North Central (1) → East (3) → Coast (7). The other path is North (2) → West (5) →South Central (4) → Coast (7). As the generation in area 2 increased, area 6 no longer exports power to area 2. Instead, area 2 exports power to area 6. Figure 5-3 shows the voltage magnitude comparison for the base case and the critical case with area interchange control on. It is obvious that the voltage magnitudes drop when the system load is increased.

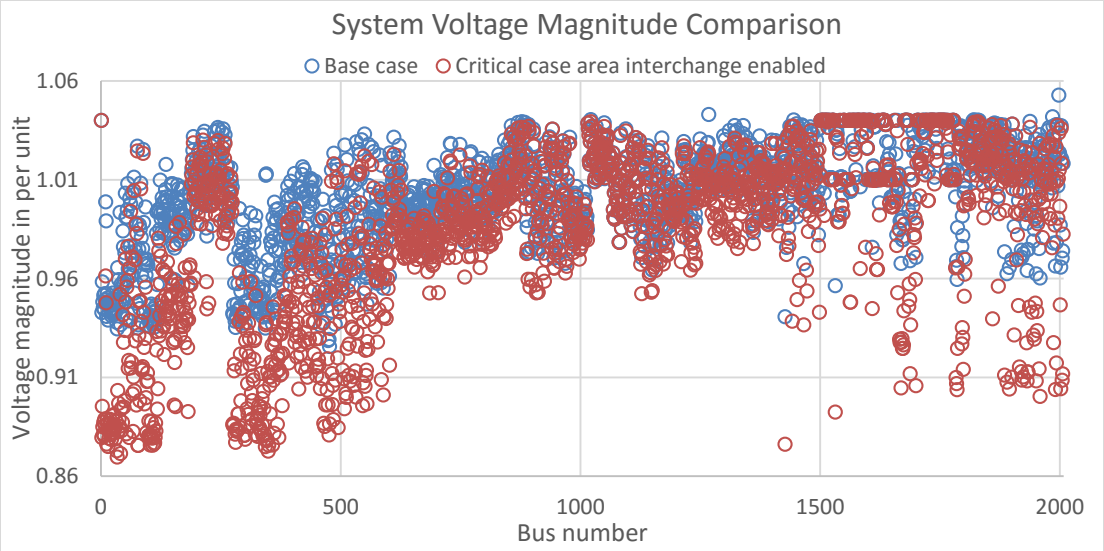

Figure 0-3 System Voltage Magnitude Comparison

The voltage magnitude comparisons between the base case and the critical case for area 1, area 2, area 5 and area 7 are given in Figure 5-4, Figure 5-5, Figure 5-6 and Figure 5-7, respectively.

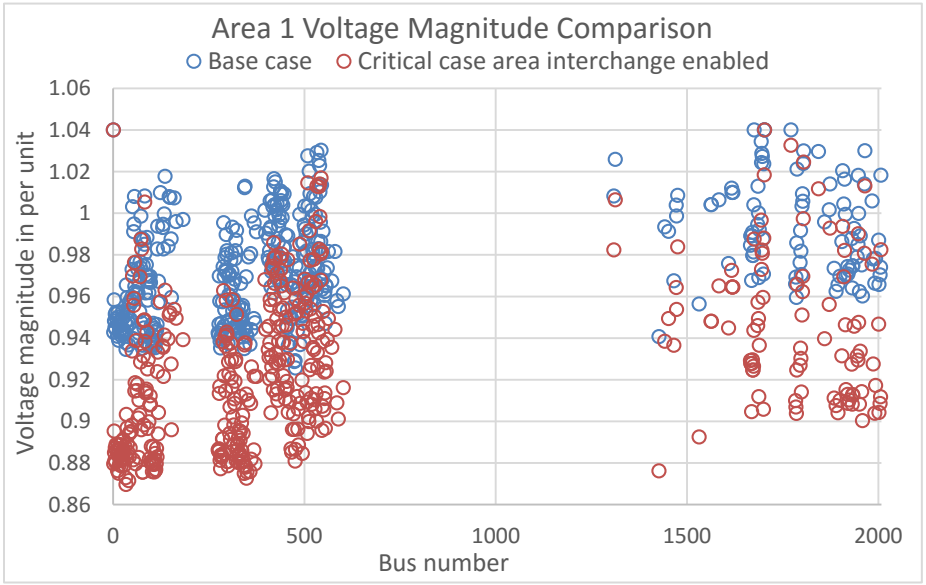

Figure 0-4 Area 1 Voltage Magnitude Comparison

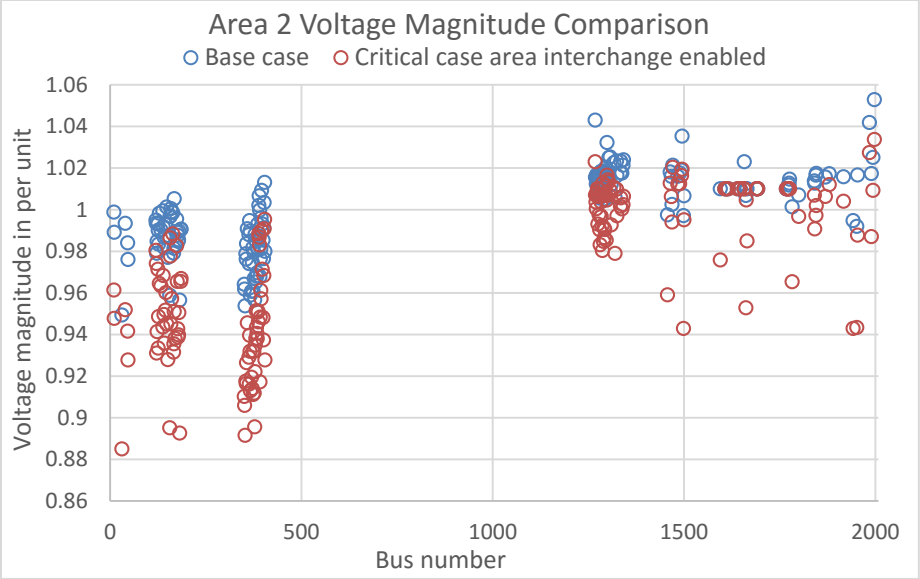

Figure 0-5 Area 2 Voltage Magnitude Comparison

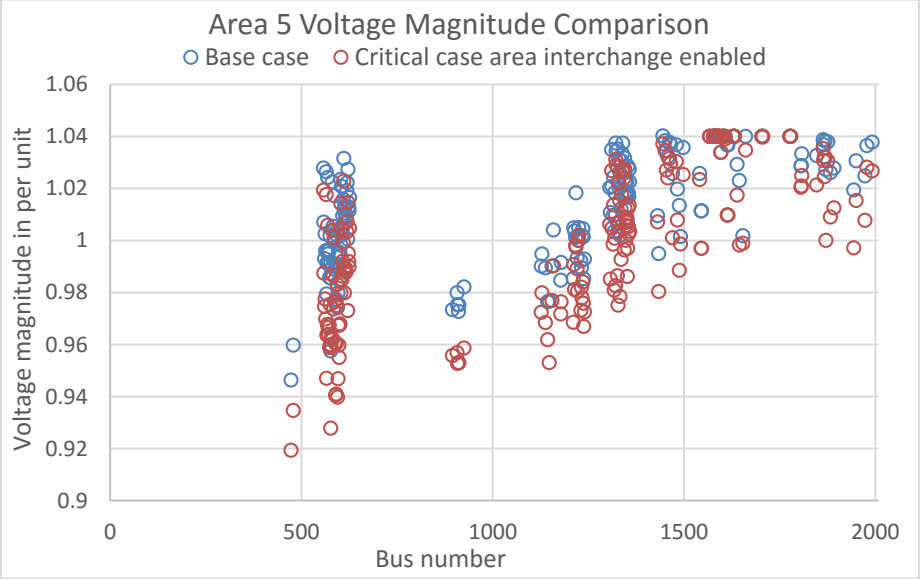

Figure 0-6 Area 5 Voltage Magnitude Comparison

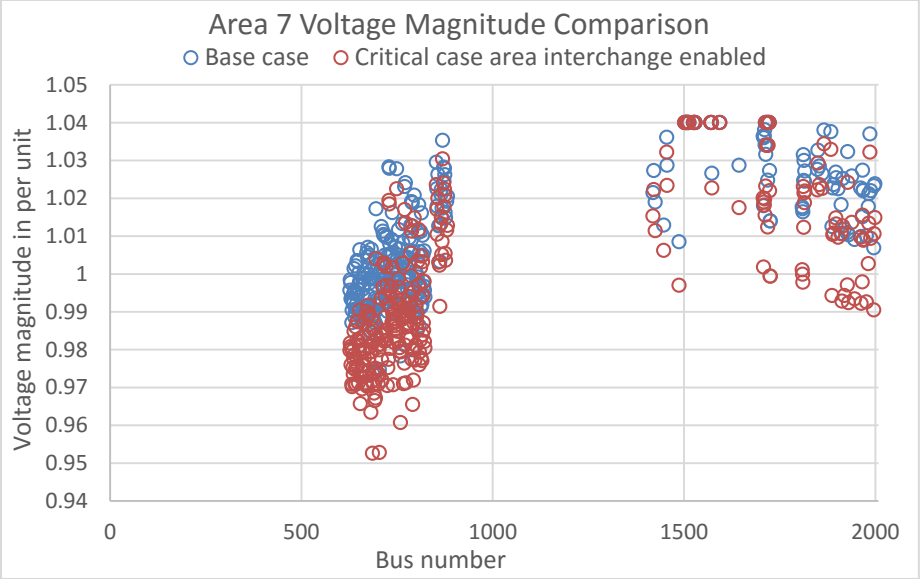

Figure 0-7 Area 7 Voltage Magnitude Comparison

Most of the low voltage magnitude buses are in area 1. Since 35 out of 36 generators are at their VAr limits in area 1, there is no more reactive power margin available to maintain the voltage magnitudes in the normal operating range. In area 2, the generator buses can hold their voltage magnitudes at nominal values. But the reactive power is inadequate to support the PQ buses, some low voltage magnitudes at PQ buses are observed in area 2. In general, the decrease in voltage magnitudes in area 1 and area 2 are more severe than area 5 and area 7.

The modal analysis for the critical case with area interchange control on gives the smallest eigenvalue to be 0.043436. The results for mode 1 are shown in Table 5-11. In mode 1, 339 buses have bus participation factor larger than 0.2. Most of them belong to area 1 and area 2, which implies that the area 1 and area 2 are weak areas of the system.

Table 0-11 Modal Analysis with Area Interchange on

No.	Bus	Gen	Area	Part.Fac.	Voltage
1	1668	QL	1	1.00000	0.9277
2	1532	QL	1	0.90498	0.8924
3	1667	QL	1	0.73317	0.9277
4	6		1	0.73225	0.8873
5	350		1	0.73006	0.8756
6	31		2	0.72860	0.8850
7	182		2	0.72625	0.8926
8	346		1	0.72114	0.8779
9	156		2	0.71956	0.8951
10	34		1	0.71764	0.8696
11	1670	QL	1	0.71536,	0.9277
12	153		1	0.71433	0.8959
13	154		3	0.71201	0.9175
14	344		1	0.71070	0.9366
15	362		1	0.69840	0.9261
16	368		1	0.69788	0.8862
17	347		1	0.69745	0.8784
18	345		1	0.69705	0.9376
19	36		1	0.69545	0.8824
20	181		3	0.69533	0.9250

5.2.2 Area Interchange Off

Table 5-12 shows the power transfer differences between the critical case with area interchange control on and critical case with the area interchange control off. Both the absolute values of the differences and percentage differences are given. The bold values show that the power transfer in the critical case with area interchange control on is increased compared to the critical case with area interchange control off. The unbolded values show that the power transfer in the critical case with area interchange control on is decreased compared to the critical case with area interchange control off.

Table 0-12 Power Transfer Difference II

From Area \ To Area	1	2	3	4	5	6	7	8
1			-136.57MW -8.8%					
2	**79.71MW 3.0%**		**0.14MW 0.3%**		-4.34MW -0.7%	-7.99MW -20.6%		
3				-15.77MW -17.6%			-71.96MW -1.8%	
4	**1.16MW 0.5%**						**10.34MW 0.4%**	
5	**76.83MW 5%**			-1.63MW -0.01%				-0.42MW -0.5%
6					**1.98MW 0.1%**			
7								
8				-0.85MW -0.1%			**2.53MW 0.3%**	

Voltage magnitude are compared in Figure 5-8 for the critical case with the area interchange control on and off.

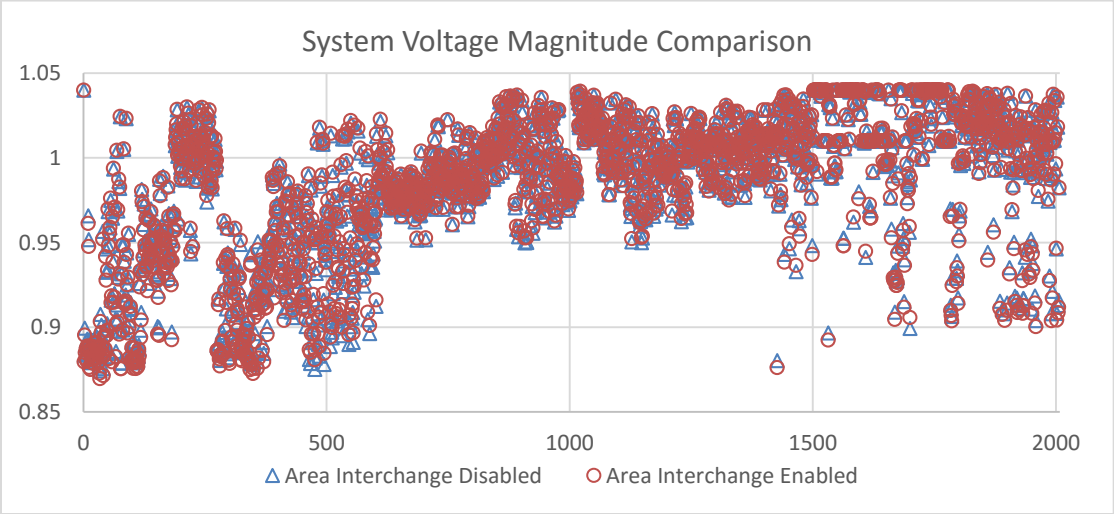

Figure 0-8 System Voltage Magnitude Comparison

As shown in the Table 5-12 and Figure 5-8, there are only some small differences between these two cases. Since more power is transferred through area 1 when the area interchange control is disabled, the voltage magnitudes drop lower as shown in Figure 5-9. Area 2 exports less power to other areas when the area interchange control is disabled, which causes a slight increase in voltage magnitudes as shown in Figure 5-10.

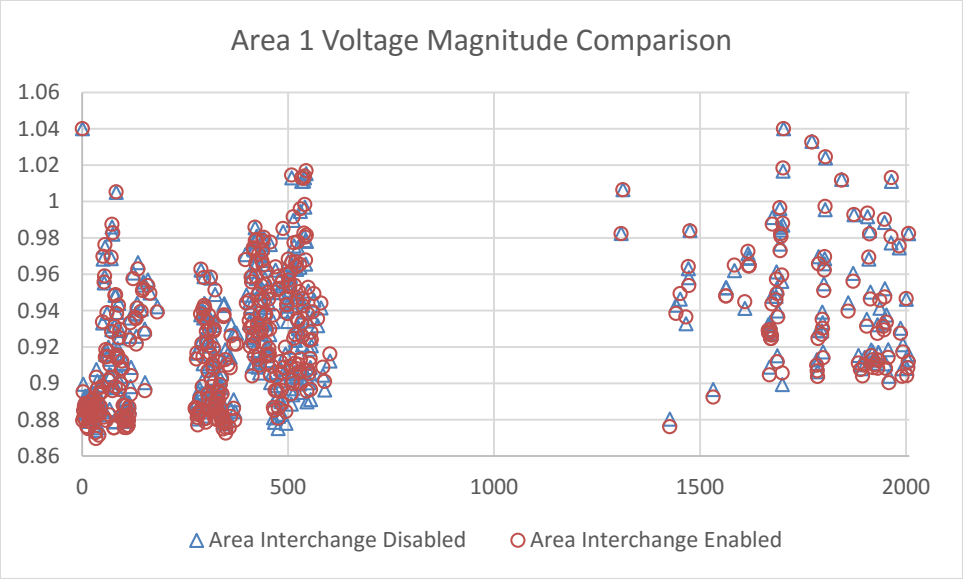

Figure 0-9 Area 1 Voltage Magnitude Comparison

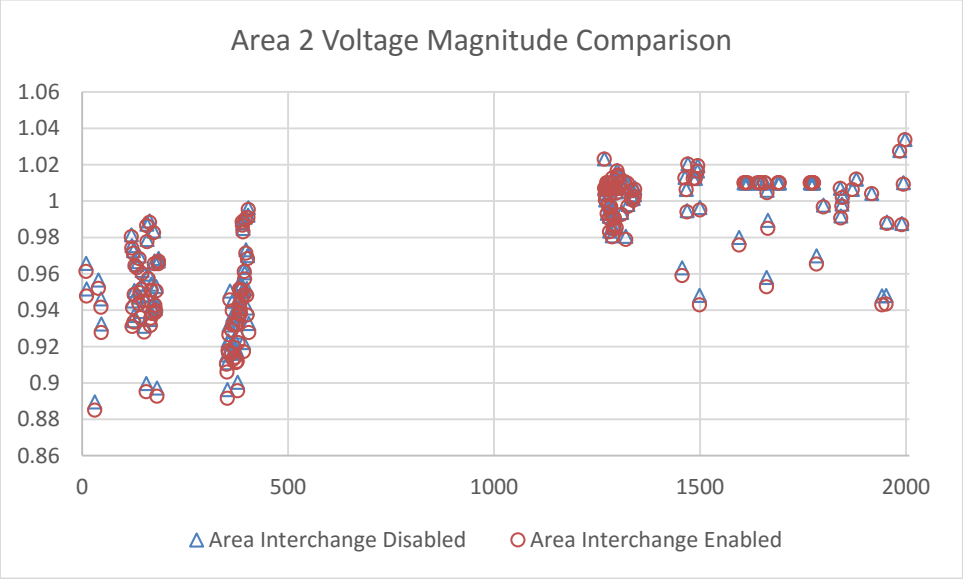

Figure 0-10 Area 2 Voltage Magnitude Comparison

The modal analysis for the critical case with the area interchange control off gives the smallest eigenvalue of 0.060956. The results are shown in Table 5-13.

Table 0-13 Modal Analysis with Area Interchange off

No.	Bus	Gen	Area	Part.Fac.	Voltage
1	1668	QL	1	1.00000	0.9318
2	1532	QL	1	0.87372	0.8966
3	1667	QL	1	0.69926	0.9318
4	1670	QL	1	0.67997	0.9318
5	6		1	0.67570	0.8919
6	31		2	0.67205	0.8896
7	154		3	0.67127	0.9213
8	350		1	0.67100	0.8803
9	182		2	0.67055	0.8972
10	156		2	0.66435	0.8997
11	346		1	0.66290	0.8826
12	34		1	0.65981	0.8742
13	153		1	0.65920	0.9004
14	181		3	0.65578	0.9288
15	344		1	0.64888	0.9428
16	155		3	0.64437	0.9327
17	368		1	0.64143	0.8910
18	347		1	0.64133,	0.8829
19	175		3	0.64077	0.9312
20	18		1	0.63935	0.8882

Notice that the smallest eigenvalue given here is larger than the smallest eigenvalue of the critical case with the area interchange control on. Recall that the results from chapter 4 indicate that when the system load and generation are uniformly scaled, the modal analysis result shows that the system is more stable with the area interchange control on. Hence, the relationship between the area interchange control and static voltage stability is dependent on the power transfer path and location of the generation and load pockets. When more power is transferred through the weak areas, the system is more vulnerable.

5.3 VAr Compensation

From Table 5-11, note that in the modal analysis mode 1, there are three buses in area 2 that participate significantly in this mode. They are bus 31, bus 156 and bus 182. These three buses are boundary buses that connect area 1 and area 2. In order to enhance the system static voltage stability, reactive power compensation devices can be employed. The FACTs device used in the previous study is applied in this study. At each trial, only one VAr compensation was device installed. Table 5-14 gives the reactive power injection, the smallest eigenvalue from the modal analysis and the voltage magnitude changes after the compensation device is installed. For example, if the FACTs device is installed on bus 31, at the critical operating point (K = 1.10), the reactive power production is 99.34MVAr at bus 31. The smallest eigenvalue increases from 0.043436 to 0.146187. The voltage magnitude at bus 31 increased from 0.8850 per unit to 1.0002 per unit.

Table 0-14 Boundary Buses VAr Compensation

Bus	VAr Injection MVAr	Eigenvalue	Voltage With VAr
31	99.34	0.146187	0.8850/1.0002
182	79.46	0.146177	0.8926/1.0002
156	75.07	0.146175	0.8951/1.0002

The voltage magnitude comparisons are given in figure 5-11 to Figure 5-15.

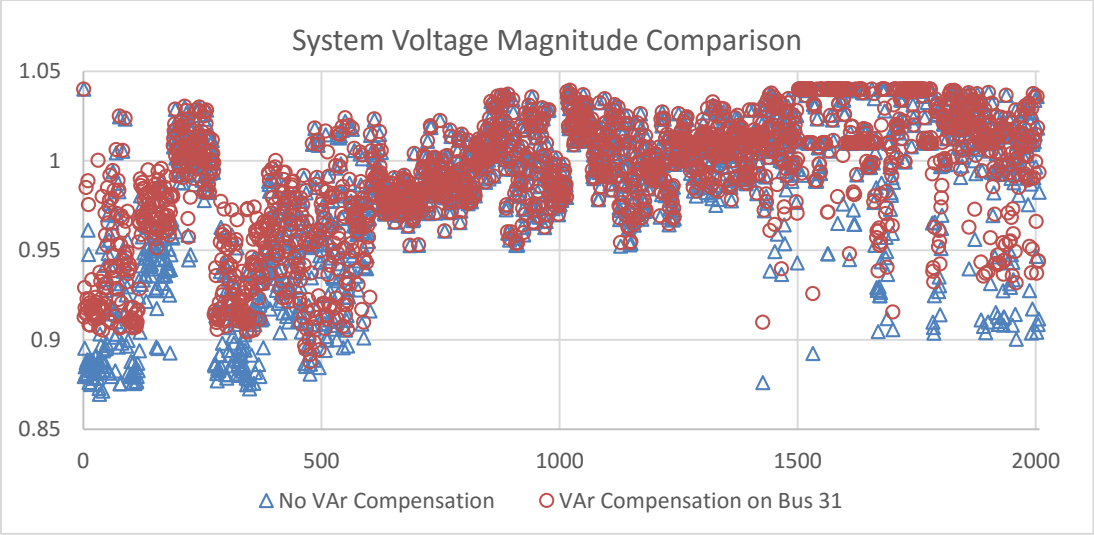

Figure 0-11 System Voltage Magnitude after VAr Compensation

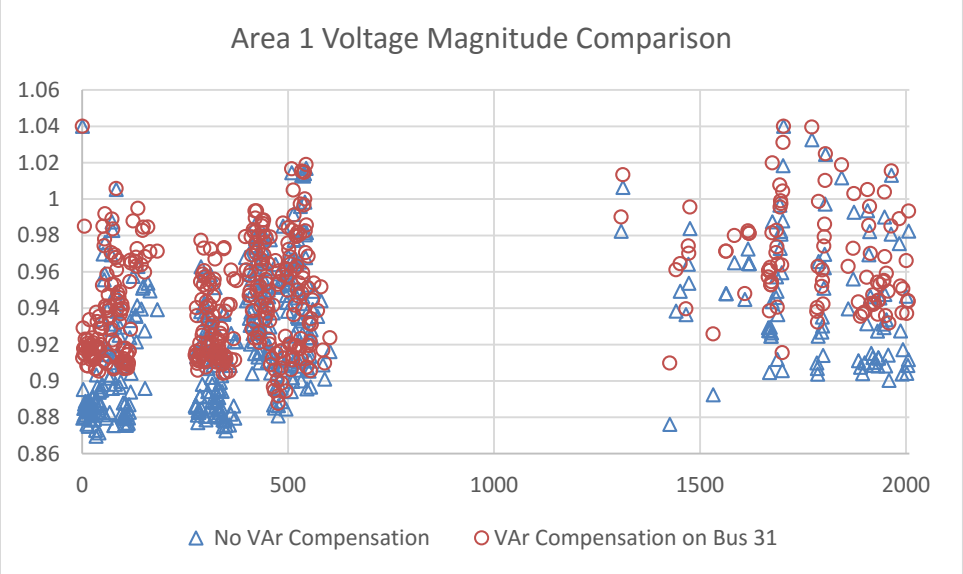

Figure 0-12 Area 1 Voltage Magnitude after VAr Compensation

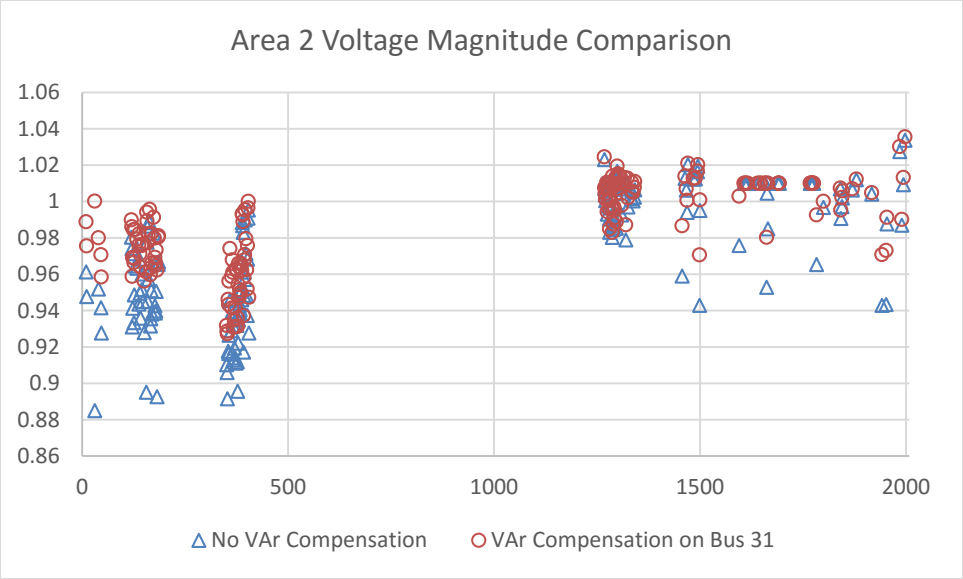

Figure 0-13 Area 2 Voltage Magnitude after VAr Compensation

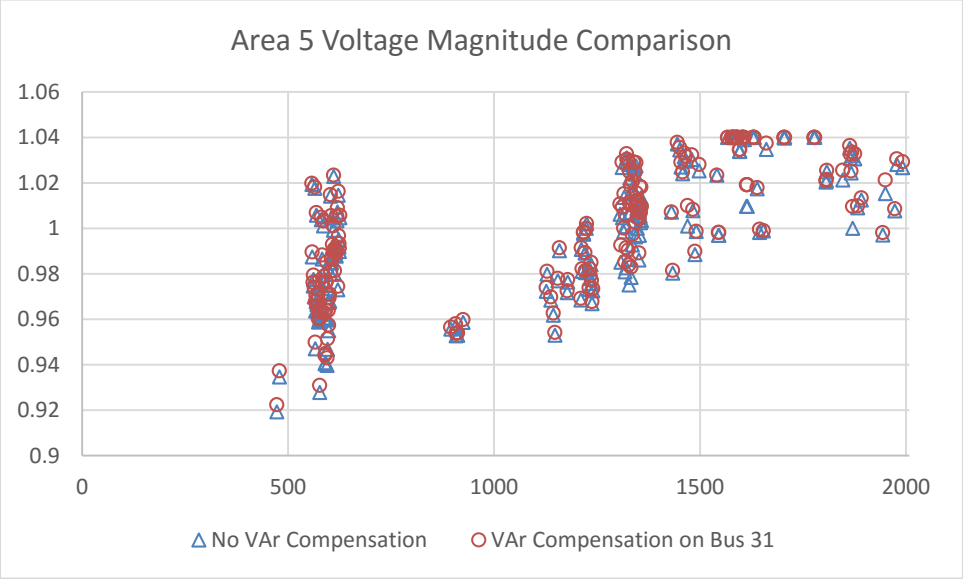

Figure 0-14 Area 5 Voltage Magnitude after VAr Compensation

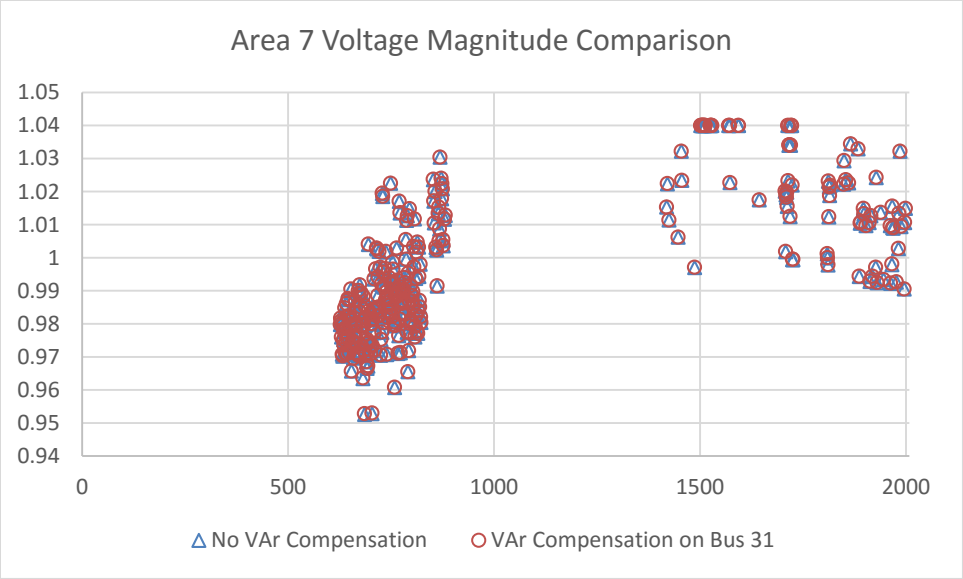

Figure 0-15 Area 7 Voltage Magnitude after VAr Compensation

As shown in the figures above, after the reactive power compensation device is installed at Bus 31, significant voltage magnitude improvements are achieved in the low voltage areas, especially in area 1 and area 2. The 99.34 MVAr reactive power provided at the single bus boosts the system voltage magnitudes significantly, and verifies that the modal analysis effectively identifies the system weak bus. When K=1.1, the reactive power injection after the VAr compensation device is installed are given in Table 5-15. The eigenvalues show that the system is more stable; even the value of K increased by 0.01, which represents an additional 142.2MW load in area 7. This also proves that modal analysis can identify the weak buses in the system.

Table 0-15 Boundary Buses VAr Compensation at the Critical Point

	K	VAr injection MVAr	Eigenvalue
31	1.11	112.11	0.107002
182	1.11	94.96	0.092904
156	1.11	91.25	0.089303

5.4 *P-V* Curves and *V-Q* Curves

Based on the modal analysis results, area 1 and area 2 are weak areas of the system. Bus 31 has the largest bus participation factor in the mode 1 at the critical case. Bus 34 has the lowest voltage in Table 5-11 and Table 5-13. The generator at bus 1676 has the largest capacity among all mode 1 generators and this generator exhausts it VAr capability at the critical case. These buses are identified as the critical buses and their *P-V* curves and *V-Q* curves are plotted to determine the static loadability limit.

5.4.1 *P-V* Curves

In the *P-V* curves, the total load in area 7 is used as the abscissa, the bus voltage magnitude of the critical buses is used as the ordinate. The *P-V* curves for Bus 31, Bus 34 and Bus 1676's are plotted in Figure 5-16, Figure 5-17 and Figure 5-18, respectively.

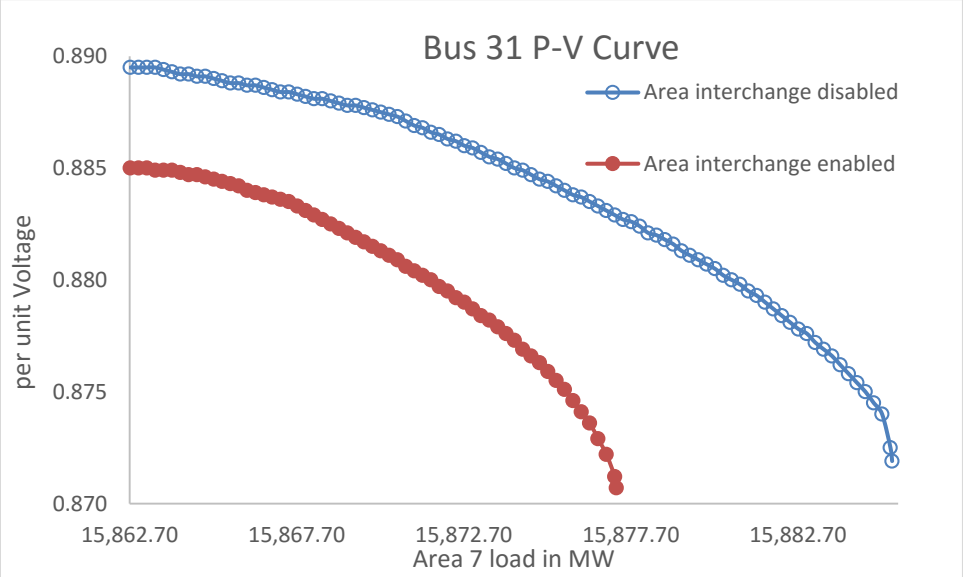

Figure 0-16 Bus 31 *P-V* Curve

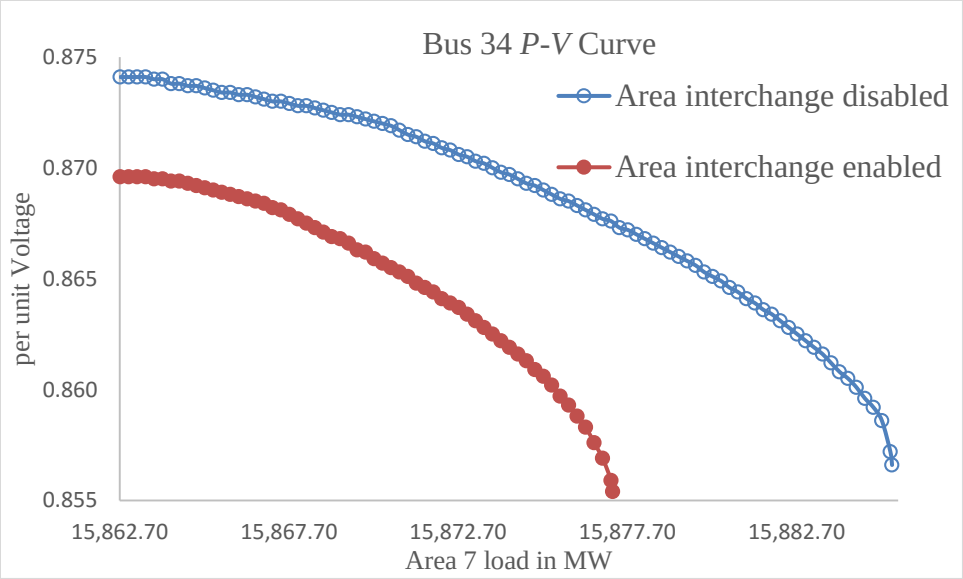

Figure 0-17 Bus 34 *P-V* Curve

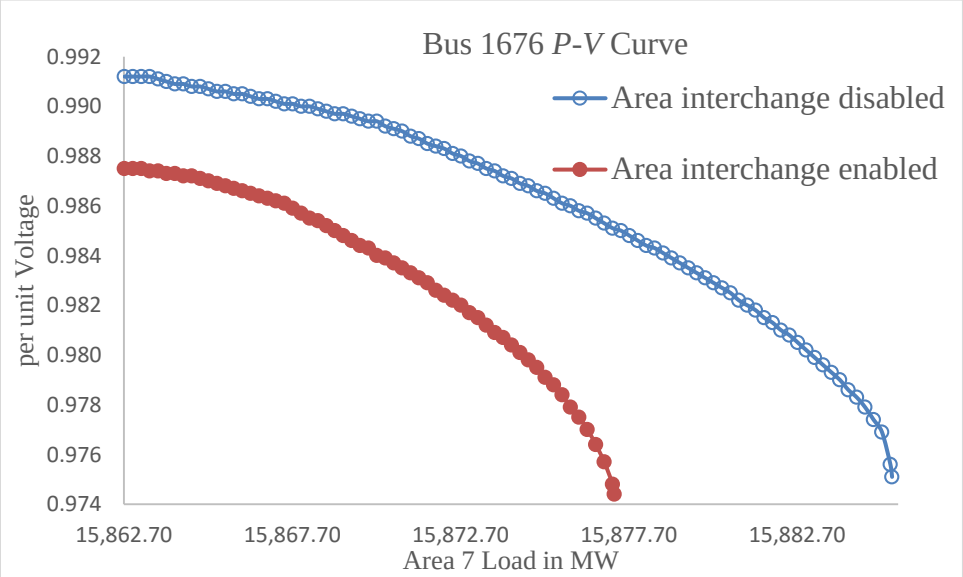

Figure 0-18 Bus 1676 *P-V* Curve

A large $\frac{dV}{dP}$ indicates that the bus voltage will drop rapidly with the load increase. At the nose point, the slope of the *P-V* curve is infinite. As shown in the *P-V* plots, the slope of the *P-V* curves are close to infinity at the critical points (the last point at which the power flow solution was obtained and modal analysis verified that the critical eigenvalue was

close to zero). After the VAr compensation device is installed at bus 31, the *P-V* curves are almost horizontal as shown in Figure 5-19. The system transfer limit is increased significantly by adding this VAr compensation device.

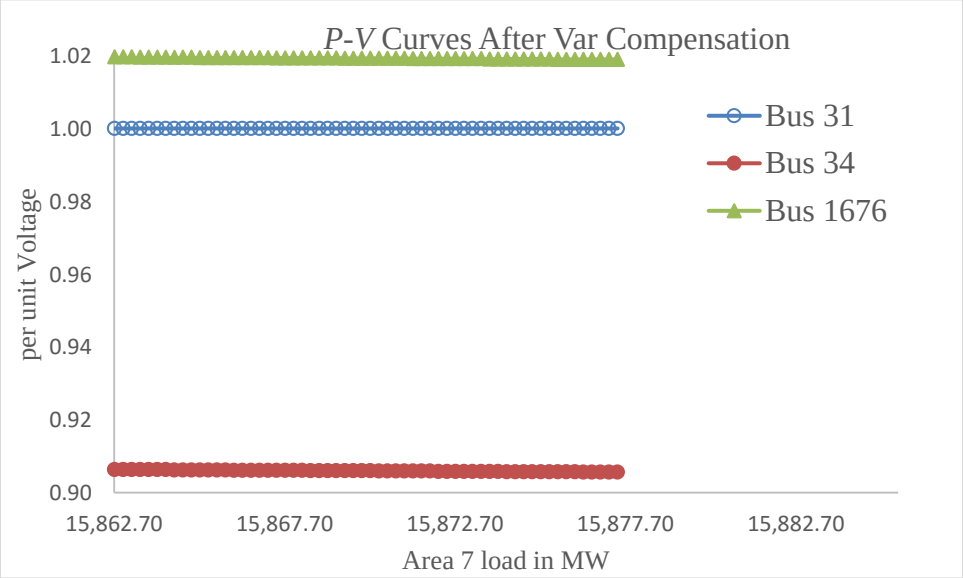

Figure 0-19 *P-V* Curve with VAr Compensation

5.4.2 *V-Q* Curves

The *V-Q* curve is often plotted by incorporating a fictitious generator whose active power output is set to zero at the desired bus. A series of power flow simulation are performed to find the reactive power generation at different bus voltage magnitude levels. At the bottom of the *V-Q* curves, $\frac{dQ}{dV}$ becomes zero which indicates the stability limit is reached. A negative $\frac{dQ}{dV}$ implies that even with additional reactive power injected, the bus voltage magnitude will drop. At the right hand side of the bottom of the *V-Q* curves, the bus is considered to be in a voltage stable operating range. Besides indicating the voltage stability limits, *V-Q* curves also provide the minimum reactive power requirement for a

steady state operation [36]. The *V-Q* curves for Bus 31, Bus 34 and Bus 1676's at *K*=1.10 are plotted in Figure 5-20, Figure 5-21 and Figure 5-22, respectively.

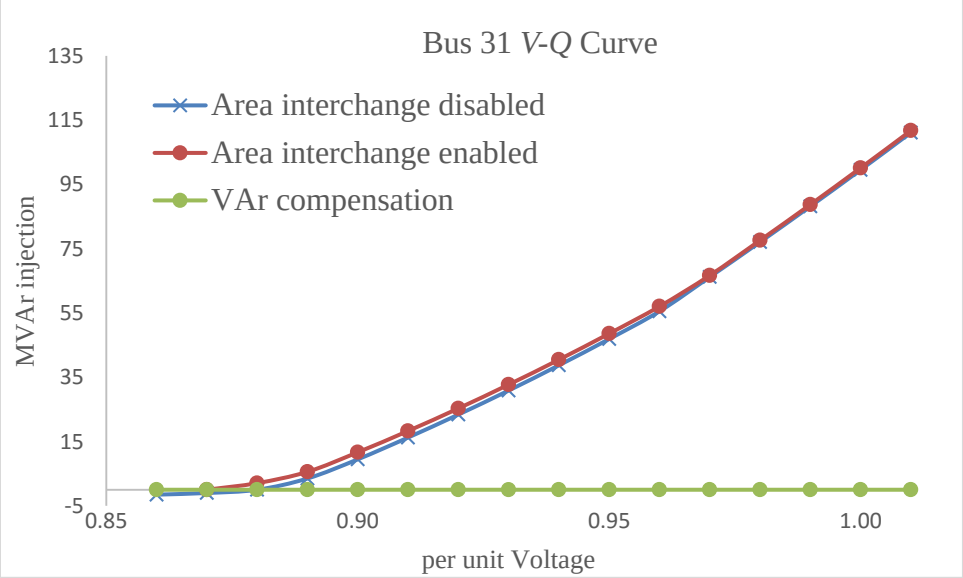

Figure 0-20 Bus 31 *V-Q* Curve

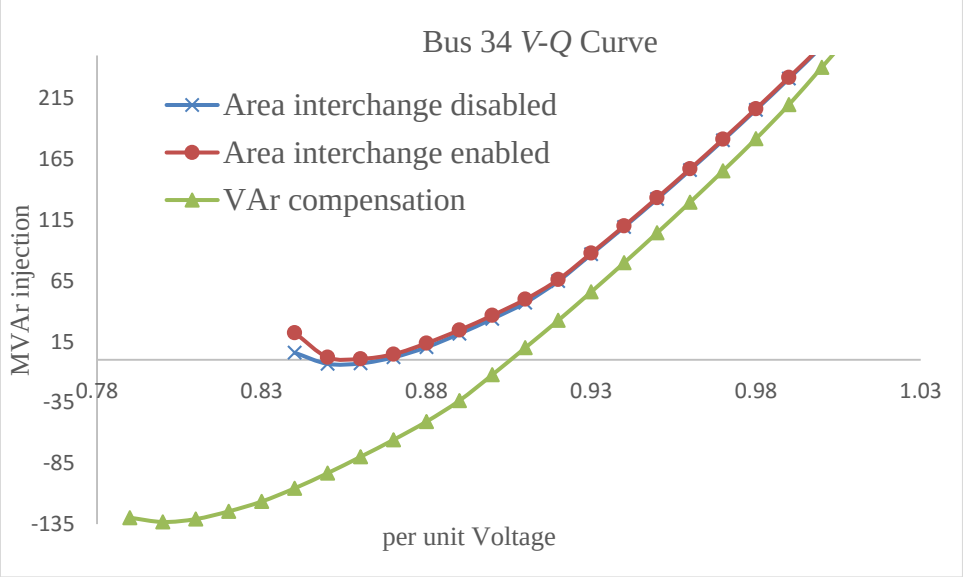

Figure 0-21 Bus 34 *V-Q* Curve

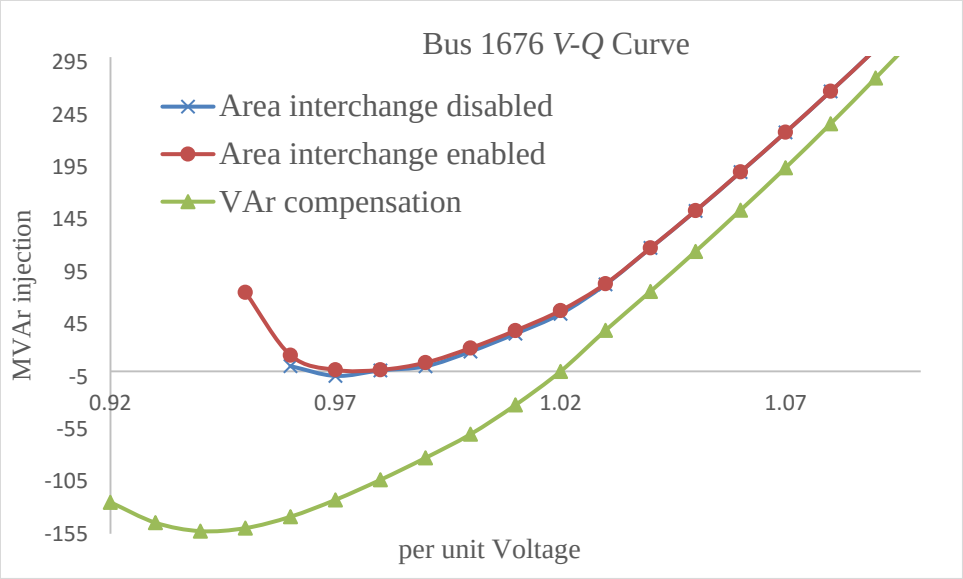

Figure 0-22 Bus 1676 *V-Q* Curve

As shown in the figures above, when the area interchange control is disabled, the system is slightly more stable compared to the area interchange is enabled. This inference coincides with that obtained from the *P-V* curves and the modal analysis results. After the VAr compensation device is installed, the *V-Q* curves move to the left hand side which indicates the reactive power margins are increased and the voltage stability is enhanced.

5.5 Summary

When the area interchange option is invoked, the desired export values should be chosen appropriately to reach a steady state operating condition. The area interchange control may require more iterations to reach the converged solution. The relationship between the area interchange control and static voltage stability depends on the power transfer paths. When more power is transferred through the weak areas, the system will be more vulnerable.

CHAPTER 6

CONCLUSIONS

This study investigated the strengths that lie in the different power flow solution techniques from different software packages. As for the conventional power flow solution techniques, the Gauss method is more robust for cases which have trouble allocating reactive power and have a poor estimation of the starting point. The Gauss method tends to converge slowly when the system is getting closer to the solution. The Newton method shows a better convergence characteristic when the system is close to its true solution. However, the Newton's method may fail to converge if the system has reactive power inadequacy or a poor solution estimate is used as the starting point. The fast decoupled method uses an almost unchanged Jacobian to reduce the computation time in solving the power flow.

As the system approaches its voltage stability limits, the Jacobian becomes increasingly ill-conditioned and may become numerically singular. The conventional power flow techniques may have convergence difficulties. One approach to overcome this issue is to use other power flow techniques such as CPF and HEM. CPF uses a path-following continuation method to overcome the singularity of the Jacobian. HEM uses a non-iterative method to guarantee the solution up to the voltage collapse point. These two methods show great potential to overcome the singularity issue near the saddle-nose bifurcation point, but immature control algorithms may cause control adjustment oscillatory behavior and lead to convergence failures. Another approach to overcome this issue is to investigate the impact of the power flow solution parameters and power flow control parameters such as the starting point, generator reactive power control, shunt devices control, and area

interchange control, and then select the appropriate settings and control method to find the voltage stability limits as close as possible. The following suggestions are given to obtain a converged solution with K being increased to the critical value:

Algorithm: The Newton method is the most commonly used method in power flow analysis. However, the Newton method has a locally convergent characteristic. A poor estimation of the starting point could result in convergence difficulties. Hence, occasionally the Gauss-Seidel method is used as a means to reliably start the power flow solution. Then, after a few iterations, the algorithm is switched from the Gauss-Seidel method to the Newton method or to the fast-decoupled method. In some applications, if only a good approximation of the solution and less computation time are needed, the fast decoupled can be applied.

Starting point: For an iterative method, a poor starting point can cause a failure in convergence or converge to a low voltage solution. A starting point based on previous solutions in cases where parameters are gradually increased to obtain limits is always favorable to a flat start.

VAr limits and bus type switching: Reactive power outputs of generators always play an important role in the voltage stability study, especially under stressed conditions. At the beginning of the solution, voltage mismatches requirements may not be satisfied due to that difficulty of allocating reactive power. It is reasonable to remove the VAr limits at the early stage of the solution and then apply the VAr limits after a few iterations.

Shunt device control: The continuous shunt control mode makes power flow solution easier to converge, but the physical shunt devices usually cannot be adjusted continuously. As the control mode is changed from continuous to discrete, there could be significant

changes in bus voltages. These can cause convergence difficulties in the solution process. Therefore, the switched shunts could be treated as continuous mode control shunts before the solution converges. Once the solution satisfies the convergence tolerance, the discrete mode shunts could be set to the nearest steps and then with this fixed value to resolve the case.

Area interchange: When the area interchange option is invoked, the desired export values should be chosen appropriately to reach an acceptable steady state operating condition. When more power is transferred through the weak areas, the system will be more vulnerable.

HEM weak bus determination can provide a good estimation of the voltage collapse point. Once the critical *K* is found, another line of this study has been to identify the weak areas of the system. The modal analysis approach is applied at the critical case to find the mode of the system voltage instability and to identify the potential weak areas and weak buses. Then *P-V* analysis and *V-Q* analysis are conducted to verify the modal analysis results.

REFERENCES

[1]. P. Kundur *et al*, "Definition and classification of power system stability IEEE/CIGRE joint task force on stability terms and definitions," *IEEE Trans. Power Systems*, vol. 19, pp. 1387-1401, 2004.

[2]. C. W. Taylor, *Power system voltage stability*, McGraw-Hill, 1994.

[3]. T. Van Cutsem, C. Vournas, *Voltage stability of electric power systems*, Kluwer, 1998.

[4]. P. Kundur, *Power system stability and control*, McGraw Hill, 1994.

[5]. J. Deuse, M. Stubbe, "Dynamic simulation of voltage collapses," *IEEE Trans. Power Systems*, vol. 8, pp. 894-904, 1993.

[6]. C. Lemaitre *et al*, "An indicator of the risk of voltage profile instability for real-time control applications," *IEEE Trans. Power Systems*, vol. 5, pp. 154-161, 1990.

[7]. B. Gao, G. K. Morison and P. Kundur, "Towards the development of a systematic approach for voltage stability assessment of large-scale power systems," *IEEE Trans. Power Systems*, vol. 11, pp. 1314-1324, 1996.

[8]. G. K. Morison, B. Gao and P. Kundur, "Voltage stability analysis using static and dynamic approaches," *IEEE Trans. Power Systems*, vol. 8, pp. 1159-1171, 1993.

[9]. T. Van Cutsem, R. Mailhot, "Validation of a fast voltage stability analysis method on the Hydro-Quebec system," *IEEE Trans. Power Systems*, vol. 12, pp. 282-292, 1997.

[10]. N. Flatabo, R. Ognedal, T. Carlsen, "Voltage stability condition in a power transmission system calculated by sensitivity methods," *IEEE Trans. Power Systems*, vol. 5, pp. 1286-1293, 1990.

[11]. B. H. Chowdhury, C. W. Taylor, "Voltage stability analysis- V-Q power flow simulation versus dynamic simulation," *IEEE Trans. Power Systems*, vol. 15, pp. 1354-1359, 2000.

[12]. B. Gao, G. K. Morison, and P. Kundur, "Voltage stability evaluation using modal analysis," *IEEE Trans. Power Systems*, vol. 7, pp. 1529-1542, 1992.

[13]. J. B. Ward, H. W. Hale, "Digital computer solution of power-flow problems," *AIEE Trans. (Power Apparatus and Systems)*, vol. 75, pp. 398-404, 1956.

[14]. W. F. Tinney, C. E. Hart, "Power flow solution method by Newton's method," *IEEE Trans. Power Apparatus and System*, vol. 86, pp. 1449-1460, 1967.

[15]. B. Stott, O. Alsac, “Fast decoupled load flow,” *IEEE Trans. Power Apparatus and System*, vol. 93, pp. 859-869, 1974.

[16]. M. Cepin, *Assessment of power system reliability: methods and applications*, Springer, 2011.

[17]. R. van Amerongen, “A general-purpose version of the fast decoupled loadflow,” *IEEE Trans. Power Systems*, vol. 4, pp. 760-770, 1989.

[18]. Siemens, PSSE Program Operatiron Manual, Schenectady, NY, USA, Siemens Industry Inc., 2015.

[19]. Powertech, Powerflow & Short-circuit Analysis Tool (PSAT) User Manual. Surrey, BC. Canada, Powertech Labs Inc., 2016.

[20]. PowerWorld Manual, [Online]. Available from: https://www.powerworld.com/WebHelp.

[21]. S. D. Rao *et al*, “The Holomorphic Embedding Method Applied to the Power-Flow Problem,” *IEEE Trans. Power Systems*, vol. 31, pp. 3816-3828, 2016.

[22]. S. D. Rao, D. Tylavsky, Y. Feng, “Estimating the saddle-node bifurcation point of static power systems using the holomorphic embedding method,” *International Journal of Electrical Power & Energy System*, vol. 84, pp. 1-12, 2017.

[23]. H. Stahl, “On the convergence of generalized Padé approximants,” Constructive Approximation, vol. 5, pp. 221-240, 1989.

[24]. H. Stahl, “The convergence of Padé approximants to functions with branch points,” *Journal of Approximation Theory*, vol. 91, pp. 139-204, 1997 .

[25]. Illinois Center for a Smart Electric Grid, IEEE 300-Bus System, [Online]. Available from http://icseg.iti.illinois.edu/ieee-300-bus-system.

[26]. Illinois Center for a Smart Electric Grid, Synthetic Power Cases, [Online]. Available from http://icseg.iti.illinois.edu/synthetic-power-cases.

[27]. V. Ajjarapu, C. Christy, “The continuation power flow: a tool for steady state voltage stability analysis,” *IEEE Trans. Power Systems*, vol. 7, pp. 416-423, 1992.

[28]. E. Allgower and K. Georg, *Introduction to numerical continuation methods*, SIAM, 2003.

[29]. V. Ajjarapu, *Computational techniques for voltage stability assessment and control*, Springer, 2007.

[30]. W.C. Rheinblodt, “Solutions fields of nonlinear equations and continuation methods,” *SIAM J. Numer. Anal.*, vol. 17, pp. 221-237, 1979.

[31]. Federico Milano, Power System Analysis Toolbox, [Online]. Available from http://faraday1.ucd.ie/psat.html.

[32]. P. W. Sauer, M. A. Pai, “Power system steady-state stability and the load-flow Jacobian,” *IEEE Trans. Power System*, vol. 5, pp. 1374-1383, 1990.

[33]. General Electric, PSLF User’s Manual, General Electric international Inc., 2016.

[34]. ERCOT, Long-term system assessment for the ERCOT region 2012, [Online]. Available from http://www.ercot.com/content/news/presentations/2013.

[35]. ERCOT, ERCOT grid information, [Online]. Available from http://generationhub.com/2014/05/14/calpine-nrg-say-ercot-project-favors-grid-upgrades.

[36]. CIGRE Task Force, “Planning against voltage collapse,” *Electra*, no. 111, pp. 55-57, 1987.